# Laser Impulse Coupling Measurements at 400fs and 80ps using the LULI Facility at 1057nm Wavelength

C. R. Phipps[1], M. Boustie[2], J.-M. Chevalier[3], S. Baton[4], E. Brambrink[4] L. Berthe[5], M. Schneider[5],  L. Videau[6], S. A. E. Boyer[7] and S. Scharring[8]

[1]Photonic Associates, LLC, Santa Fe, USA, [2]CNRS-ENSMA, U. Poitiers, Futuroscope, France, [3]CEA, DAM CESTA, Le Barp, France, [4]LULI, CNRS-École Polytechnique-CEA-UPMC, Palaiseau, France, [5]CNRS-Arts et Metiers ParisTech, Paris, France, [6]CEA, DAM, DIF Arpajon, France, [7]Mines ParisTech, CEMEF, Sophia Antipolis, France, [8] DLR, Stuttgart, Germany

## Abstract

At the École Polytechnique « LULI » facility, we have measured the impulse coupling coefficient $C_m$ (target momentum per joule of incident laser light) with several target materials in vacuum, at 1057nm and 400fs and 80ps pulse duration. A total of 64 laser shots were completed in a two-week experimental campaign, divided between the two pulse durations and among the materials. Our main purpose was to resolve wide discrepancies among reported values for $C_m$ in the 100ps region, where many applications exist. A secondary purpose was to compare $C_m$ at 400fs and 80ps pulse duration. The 80ps pulse was obtained by partial compression. Materials were Al, Ta, W, Au and POM (polyoxymethylene, trade name Delrin). One application of these results is to pulsed laser ablation propulsion in space, including space debris re-entry, where narrow ranges in $C_m$ and specific impulse $I_{sp}$ spell the difference between dramatic and uneconomical performance. We had difficulty measuring mass loss from single shots. Imparted momentum in single laser shots was determined using pendulum deflection and photonic Doppler velocimetry. $C_m$ was smaller at the 400fs pulse duration than at 80ps. To our surprise, $C_m$ for Al at 80ps was at most 30N/MW with 30kJ/m² incident fluence. On the other extreme, polyoxymethylene (POM, trade name Delrin) demonstrated 770N/MW under these conditions. Together, these results offer the possiblity of designing a $C_m$ value suited to an application, by mixing the materials appropriately.

## 1.0 Introduction: Laser Ablation Propulsion Parameters for Short and Ultrashort Pulses

### 1.1. Challenge

The problem driving this work was the need for accurate impulse coupling parameters for practical short and ultrashort laser pulse durations, 80ps and 400fs, on common space materials. The most important of these are impulse coupling coefficient $C_m$ and the  laser-produced jet's specific impulse $I_{sp}$, a rocketry parameter related to average jet velocity $v_E$ by the standard acceleration of gravity $g_o$

$$I_{sp} = v_E/g_o .  \qquad (1)$$

$I_{sp}$ depends upon target mass loss $\delta m_T$ during each pulse because the momentum given to the target by $W$ joules of incident laser light incident is

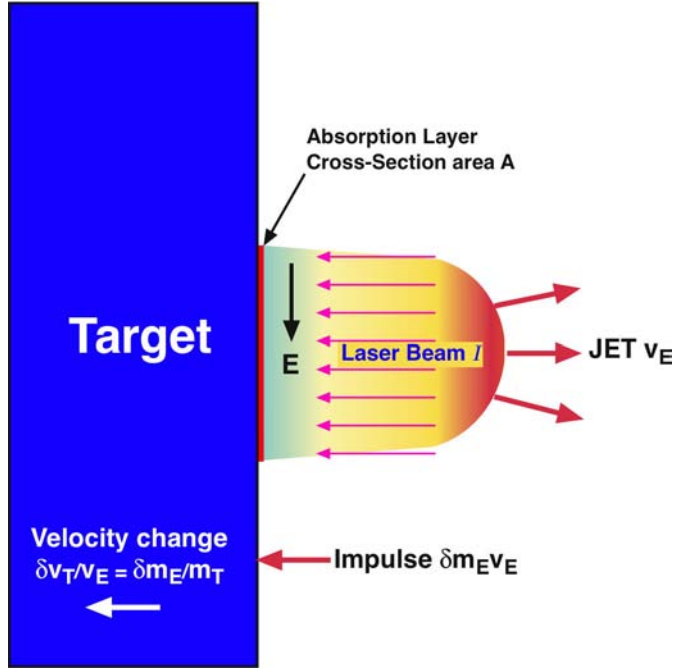$$C_m W = \delta m_T g_o I_{sp} \qquad \text{N-s.} \qquad (2)$$

[See Figure 1]. Mass conservation requires $\delta m_T = \delta m_E$.

Their product gives the thrust efficiency of the ablation process. With $\psi = \langle v_E^2 \rangle / \langle v_E \rangle^2$,

$$C_m I_{sp} = [2/(\psi g_o)] \eta_{AB}. \qquad (3)$$

We take $\psi = 1$ in this work, as explained below. This efficiency is just the ratio of the exhaust kinetic energy to incident laser energy.

Mass loss is very difficult to measure in a single pulse. To put this statement in perspective, using typical values for fluence $\Phi = 30\text{kJ/m}^2$ on target and $C_m$



**Figure 1.** Laser Ablation Impulse Generation

= 35 N/MW in an $A_s$ = 1cm² laser spot area,

$$\delta m_T = A_s C_m^2 \Phi / (2\eta_{AB}) \qquad (4)$$

is less than two nanograms in typical single short pulse interactions.

It must be understood that the Eq. (1) – (4) parameters are convenient approximations to moments of real plasma velocity distributions, as we explain more fully in the theoretical section, where we will also derive Eq. (4).

### 1.2 Brief History of Laser Ablation

The history of photon propulsion begins ninety years ago with Tsander[1], Tsiolkovskii[2] and Oberth[3], leading to today's "solar sails." In 1953, Sänger published his concept for photon rockets[4] even before the invention of lasers.

However, for usefully large forces - for example, enough to counteract gravity or accelerate a several-kg object to orbital speeds in a reasonable time, pure photon propulsion is too weak. Laser ablation propulsion (LAP), giving a $C_m$ value four to five orders of magnitude larger, was first proposed by A. Kantrowitz[5] in 1972.

Laser ablation propulsion operates, ideally in vacuum, by inducing a plasma jets from a target using a laser pulses, which transfers momentum to the target (Figure 1)[6].
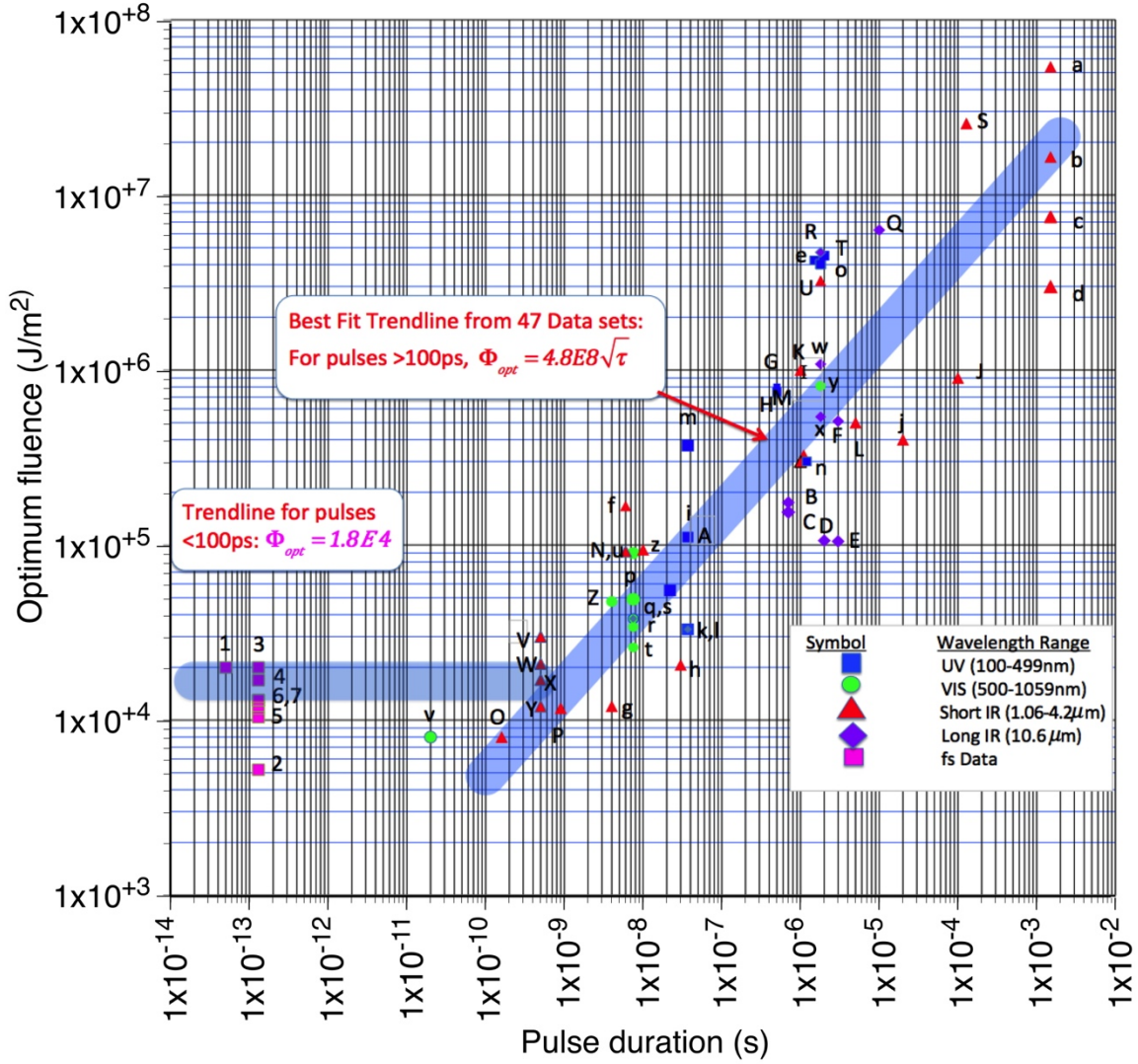
**Figure 2.** Literature values for optimum fluence across a wide range of pulse durations. On the right (pulses longer than 100ps), the trend is for $\Phi_{opt}$ to increase with the square root of pulse duration.

In Figure 2, literature references for the data listed are these: a, b, c, d: aluminum, copper, graphite, and lead[7]; e: aluminum[8]; g, h, O, P: aluminum[9]; i, k, l, m: tantalum, titanium, PMMA, and aluminum, w, x, A: aluminum, kevlar epoxy, and nylon, B, C: cellulose acetate[10]; n: aluminum[11]; o: aluminum, y: kevlar epoxy, and T, U: aluminum[12]; p, q, r, s, t, u: beryllium, graphite, aluminum, zinc, silver, and tungsten[13]; z: copper[14]; G: titanium[15]; H: aluminum and E, F: carbon phenolic and graphite[16]; I, J, K, L, M: titanium and grafoil[17]; Q: aluminum[18]; R: stainless steel[19]; S: aluminum[20]; Z, f: copper[21]; N: Al[22]; 1: Ti[23]; 2: Mo[24]; 3: W, 4: Au; 5: Li; 6: Fe and 7: glycidyl azide polymer[25]; v:Al [simulation][26]; V,W,X,Y: Al[27], [all simulations, circular polarization, $\Theta_{inc}$ = 0, 45, 60° and 75° respectively].

Even better efficiency than the continuous (CW) $CO_2$ lasers envisioned as sources by Kantrowitz is obtained with pulsed laser sources. For high efficiency in laser ablation propulsion, the laser beam must use repetitive, high intensity pulses [e.g., 20kJ, 10ps, 50Hz]. There are several reasons for this recommendation [28]. First, high $I_{sp}$ has not been demonstrated by any reliable published data with CW lasers in vacuum. Second, our calculations[29] show that the CW intensity on target needed to achieve even low values of $I_{sp}$ (about $1GW/m^2$) require a very high power laser (e.g. 1GW for a $1m^2$ target at a distance of 200km). Second, CW laser interactions have a "welding torch" problem, generating lots of low-velocity splash which quickly destroys $I_{sp}$ when compared to a 10ps pulse stream. Third, CW laser thermal coupling to the target will be disastrous because of weak plasma shielding. Last, repetitive pulses can ensure plasma clearing between shots so that it doesn't interfere with propagation.

Dozens of works have shown that ps and fs pulses give surgically clean material removal, suggesting ablation efficiency as well as low thermal coupling[30].

### 1.2.1 Short-pulse Coupling Data Prior to our Measurement Program

#### TABLE I: Existing Short Pulse $C_m$ Data (all 800nm)

| Fluence ($kJ/m^2$) | $C_{mopt}$ (N/MW) | Pulsewidth (fs) | Material | Reference no. |
|---|---|---|---|---|
| 20 | 18 | 50 | Ti | 23 |
| 5.2 | 42 | 130 | Mo | 24 |
| 20 | 40 | 130 | W | 25 |
| 17 | 85 | 130 | Au | 25 |
| 10 | 25 | 130 | Li | 25 |
| 13 | 49 | 130 | Fe | 25 |
| 13 | 25 | 130 | GAP | 25 |
| 12 | 18 | 130 | Al | 25 |

In the theoretical section, we will see that $C_m$ should vary to first order with the square root of atomic mass, other factors being constant. Table I data is quite scattered with regard to this trend. The variation of the theoretically predicted ratio $C_m/A^{0.44}$ is too great to justify a trend in this data. In Table I, GAP refers to glycidyl azide polymer, an energetic material which gave giant results in ms-pulse propulsion work.

$C_m$ is a relatively sensitive function of laser fluence delivered to the target. In the Table, $C_{mopt}$ refers to the maximum value of $C_m$ which can be obtained as fluence varies (Figure 3).

Why are there so few data? There are several reasons. First, measuring $C_m$ is an unusual interest among ultrashort physics workers, most of whom are looking for an effect other than transferred momentum, which requires specialized equipment.

Second, as we said in §1.1, it is difficult to measure mass loss with single pulses, and not so many lasers are capable of several J pulses in the fs region. We were fortunate to have the École Polytechnique "Elfie" laser available for our program.

### 1.2.2 Required Laser Fluence on Target

The main argument for short rather than long pulses is that longer pulses require progressively more pulse energy according to $\tau^{1/2}$ to reach $C_{mopt}$ [Figures 2, 3]. This feature is mainly due to the time-dependence of thermal diffusion. As a practical matter, using repetitively pulsed lasers, it is less expensive to generate a given power with small energy and high repetition rate than the reverse.
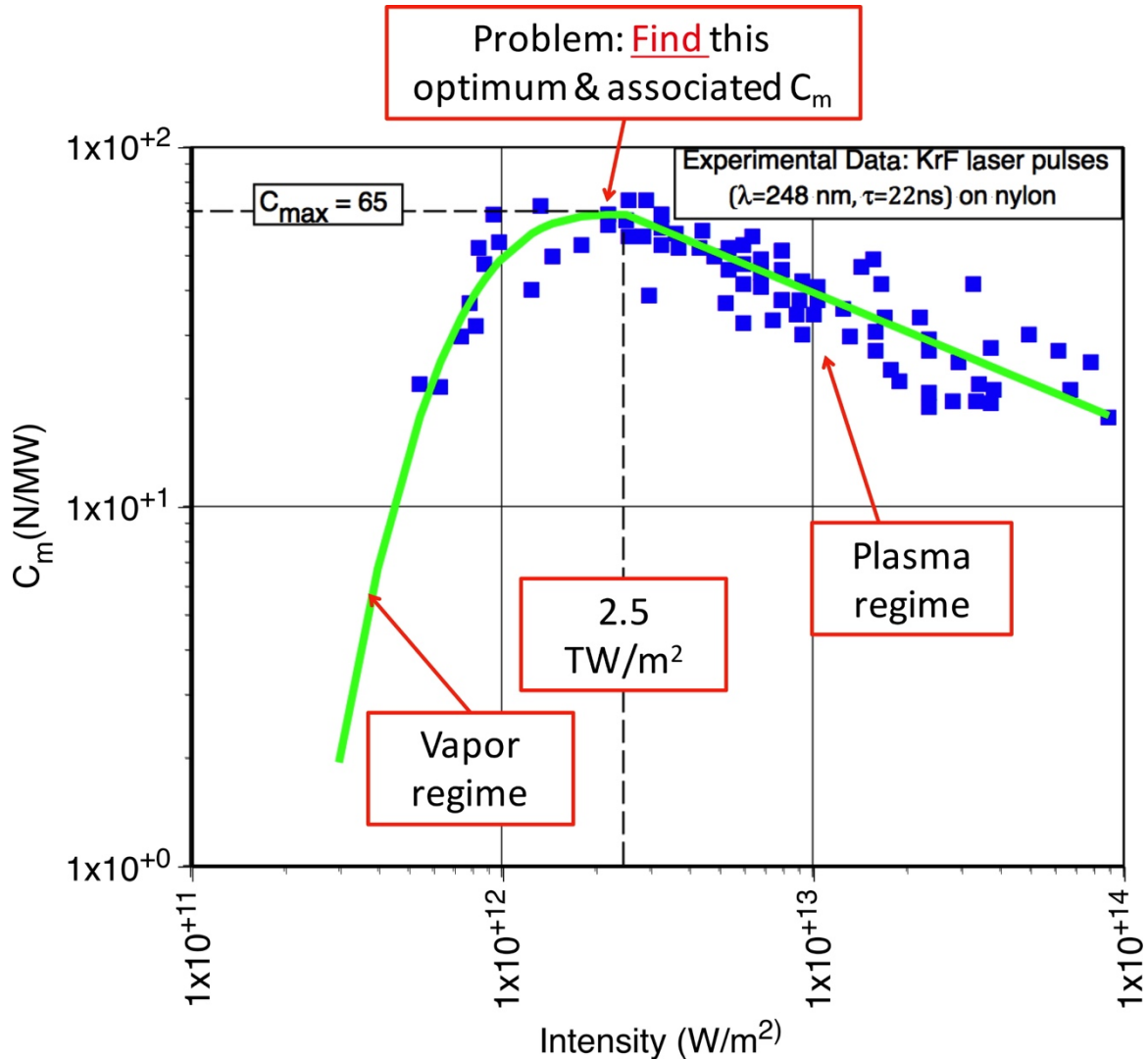


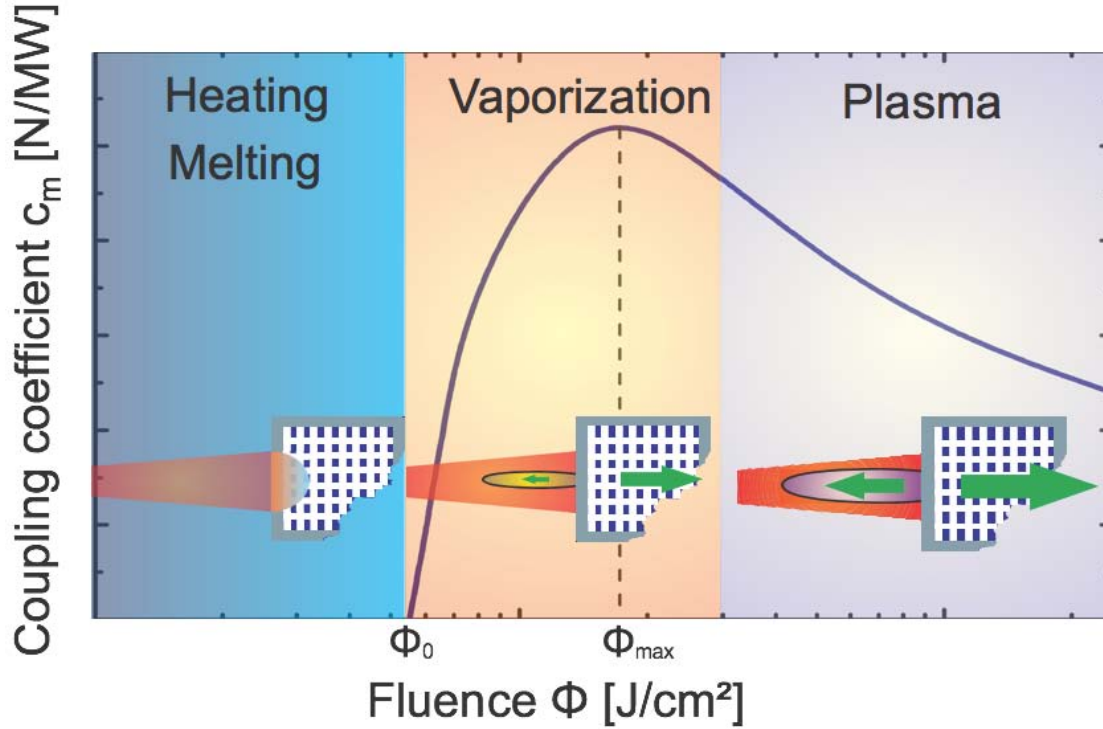**Figure 3A.** Optimum Coupling illustration

**Figure 3B.** Optimum Coupling concept

Figures 3A and 3B illustrate what is meant by optimum coupling[28, 31]. At the optimum, a rising trend in $C_m$ from vapor formation is just compensated by a declining trend due to increased laser energy required for accelerating plasma. Determining this optimum quantitatively is a complex problem which depends on target material properties and laser pulse parameters. Coupling in the plasma regime is relatively easier to predict for most passive (nonergetic) materials, such as metals and simple plastics like epoxies. Note that we need to predict not only the magnitude of $C_m$ but the fluence at which $C_{mopt}$ occurs. There is a good physical reason for $C_m$'s decline in the plasma regime: dimensionally, we can see that it varies like $1/v_E$ ($C_m$ = N-s/J = momentum/energy).

## 1.3 Important Recent Developments in Lasers and LAP Applications

**1.3.1 Development of fs fiber laser amplifiers** which can in principle be combined and phased to provide the average power (kW level) and pulse energy (100J) necessary for LAP at 100km range[323334] (the ICAN system). Phasing is a very difficult problem. Considering that pulse energy is limited to about 1mJ in fs fibers due to nonlinear optical effects[35], and that 100k fibers would be necessary to produce 100J pulses, phasing to $\lambda/10$ would be difficult for CW fibers, let alone fs-pulsed ones. To date, 64 CW fibers have been phased[36] and four fs fibers[37]. Nevertheless, if ICAN is successful, many important advantages accrue, particularly light weight, power efficiency, heat dissipation and near-instantaneous electronic beam steering.

6

### 1.3.2 Development of monolithic diode pumped solid state lasers suitable for LAP

In other work[38]we have justified the laser requirements shown in Table II.

**Table II. Laser Requirements**

| | |
|---|---|
| Type | Diode-pumped Nd |
| Wavelength | 1057nm for ground launch, 532nm in space |
| Pulse duration | 80ps |
| Pulse energy | 0.1 - 1kJ |
| Pulse repetition rate | 250Hz |
| Average power | 25 – 250kW |

Such high repetition rate, high pulse energy lasers are are not yet available, but are close to being demonstrated. The state of the art in the lasers we currently need to achieve all of these applications is represented in the HiLASE program [39], where the Rutherford Appleton Laboratory's "DiPOLE 100" laser achieved its full design performance of 1kW average power with 10Hz, 100J pulses at 10ns pulse duration. We prefer 1057nm for the wavelength in atmosphere because absorption is less than at the second and third harmonics, especially at low elevation angles. In space, 355nm is ideal. For energy storage, 6GJ, 15MW super batteries using zinc hybrid cathode technology have now been developed[40].

### 1.3.3 Exciting new applications for LAP, expanding beyond the initial concepts of

space debris removal[41][42] to spaceborne systems for small debris removal (for which LAP is the only answer) to much more advanced concepts. These include nudging large objects before a predicted collision, reorbiting defunct GEO stations, and launching 25kg objects from Earth to low Earth orbit (LEO)[43][44],[45], and from LEO to interplanetary space[46].

### 1.4 Important LAP Unknowns

The leading theory for laser impulse coupling in the plasma regime to passive absorbers like metals and epoxies[10] breaks down for pulses shorter than 100ps[47]. Can we extrapolate from the few measurements valid for longer pulses to the fs and ps regime? Extrapolation from one simulation[26] predicted $C_m$=100N/MW at 100ps[45].

What about the "supercouplers," plastics like GAP and polyoxymethylene (POM) which have demonstrated huge coupling coefficients as large as 3,000N/MW for ms pulses at 900nm and for flights using 10-um lasers [48]? None of our extrapolations predict that behavior and it is currently not understood. Do we get super coupling on POM for 80ps, $1\mu$m pulses? There is a rumored 10-$\mu$m resonance, but the same resonance can't be present at 1$\mu$m.

What is the *thermal* coupling coefficient $C_{th}$ (heat energy deposited in the substrate/incident laser energy) for fs and ps pulses? Our laser launching applications require hundreds of thousands of pulses and we must have $C_{th}$<=2% to avoid target melting. Hydrodynamic simulations predict that for ultrashort pulses at 1064nm, it can be as small as 5% or even less (see below). This unknown is very important, but not one

that we can resolve in this paper. It requires repetitively pulsed short pulse lasers with large pulse energy to resolve. Please see §8.

## 2.0 Purpose of This Work

The purpose of this work was to resolve the unknowns involving $C_m$ in the ps and fs regimes. For this purpose we required a laser with the order of 10J pulse energy and both fs and ps pulse outputs. One of the few in the world capable of this is the "Elfie" facility of École Polytechnique, Palaiseau, France. Fortunately, we obtained two weeks of beam time on Elfie to do this. This is a report of the first round of such experiments.

This facility is capable of 35TW, 1057nm pulses at 400fs (better compression), but also 12J, up to 80ps pulses (lower compression) by using the chirped, uncompressed pulse shifting from blue to red in its 6nm bandwidth. It also operates at the second harmonic, 528nm, with energy up to 5J, depending on the compression.

## 3.0 Theoretical Background

For laser space propulsion applications, it is critical to know $C_m$, which defines the laser power required to generate a force by ablating the surface of a distant target. $C_m$ varies a lot among materials, and with laser parameters. Specific impulse, $I_{sp}$, gives the lifetime of ablation fuels in laser rocket designs.

Our plasma regime theory was very successful where it applied[10]. Later work[49,50,51] treated the transition from vapor-dominated to plasma-dominated regimes and permitted estimates[52] of $C_{mopt}$ and $\Phi_{opt}$ using both SESAME tables[53] and heuristics involving ablation threshold which showed maxima at either 4.2 times[50] or 6.9 times[54] the threshold fluence. Obviously, SESAME is better where data exists over a sufficient range of temperature. In the ns pulse regime, these calculations were quite precise.

### 3.1 Fully Formed Plasma Regime Theory

In the fully formed laser produced plasma regime, the plasma itself mediates the laser plasma interaction with a solid surface. The wavelength actually reaching the solid surface will be in the hard UV, independent of the laser wavelength. This is a two-temperature problem with slow and fast ions, the latter being dragged to a high velocity by hot electrons escaping from the laser-produced plasma corona[55] [Figure 4]. There are good examples for this effect in the literature[56]. The lower ion temperature is treated in the vapor regime theory.
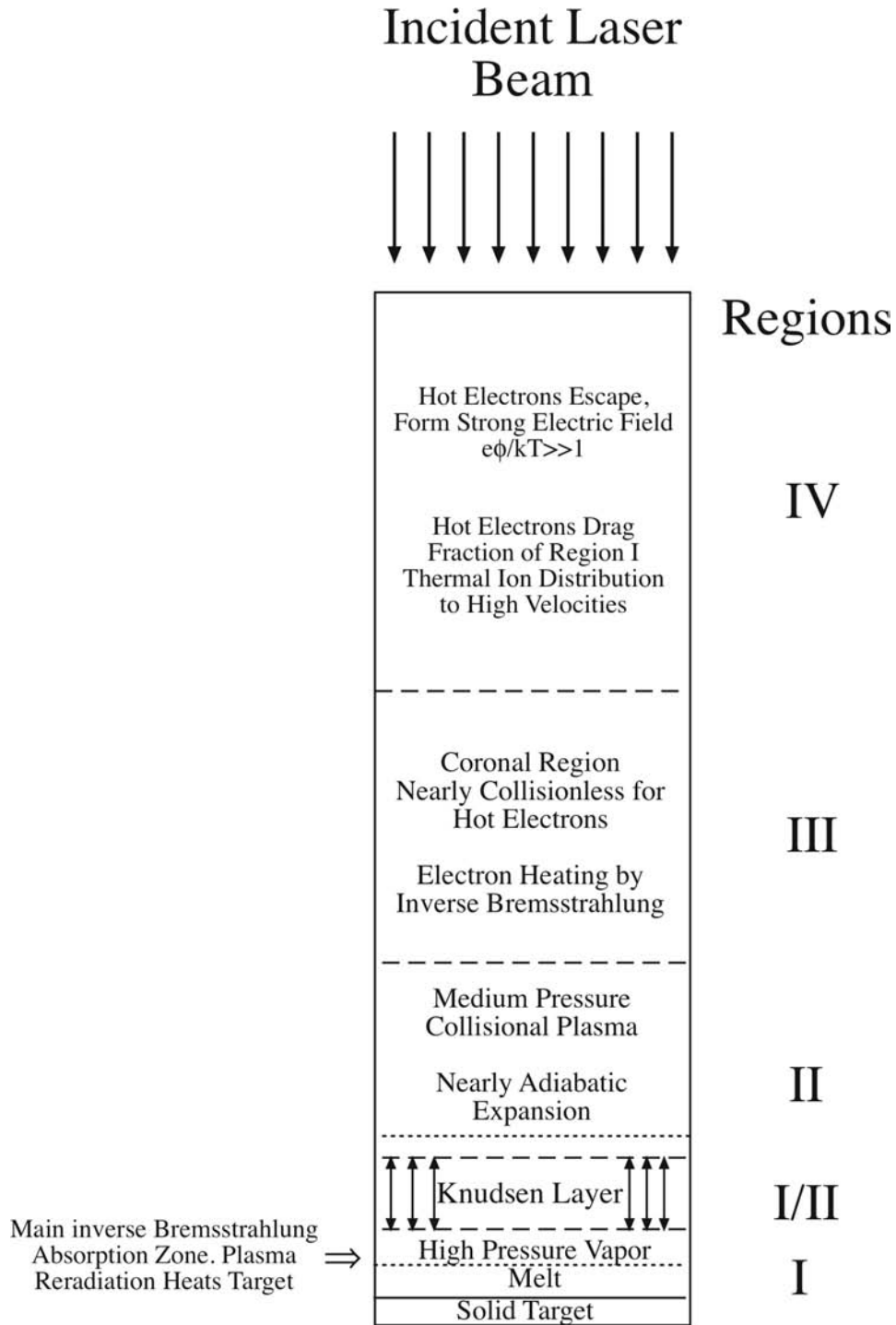
# Incident Laser Beam



**Figure 4.** Four regions of laser plasma interaction

We assume that the plume velocity distributions are drifting maxwellians with $<v_x> = u$. Throughout this work we will use $v_E$ for $<v_x>$.

Then, the 3D velocity distribution is (where $\beta = m/2kT$ and $C_x = C_y = C_z = (\beta/\pi)^{1/2}$ )

$$f(v_x, v_y v_z) = C_x C_y C_z \exp - \beta [(v_x - u)^2 + v_y^2 + v_z^2] \tag{5}$$

We have

$$<v_x^2> = \int dv_x v_x^2 f(v_x) = C_x[\pi^{1/2}/(2\beta^{3/2}) + \pi^{1/2}u^2/\beta^{1/2}] = (kT/m_E + u^2) \tag{6}$$

To gauge the consequence of substituting $<v_x^2>$ by $(<v_x>)^2$ in Eq. (3), we calculate their ratio $\psi$ from Eqs. (5) and (6) to find

$$\psi = (u^2 + kT/m_E)/u^2 \tag{7}$$

If we consider a Mach 1 ($M = u/c_s = 1$) drift velocity with sound speed $c_s = (\gamma kT/m_E)^{1/2}$, and $\gamma = C_p/C_v = 5/3$, we have $\psi = 1.60$.

However, a preponderance of measurements summarized in Phipps and Dreyfus[55] show highly pronounced forward peaking relative to the angular distribution one would obtain with $M = 1$. Where $\theta$ is the angle to the surface normal, these authors reported a $\cos^\nu\theta$ plume distribution which corresponded to $M = 2$. Then, Eq. (7) gives

$$. \qquad\qquad \psi = (4\gamma + 1)/4\gamma = 1.15 \tag{8}$$

We take $\psi = 1$, a slight error that actually underestimates $\eta_{AB}$, as can be seen in Eq. (3)..

It is clear that assigning a single temperature to the plasma plume is not very meaningful. To make the problem tractable, we use decoupled electron and ion temperatures $T_e$ and $T_i$ and make several other assumptions listed in reference 10. The salient results are as follows (subscript "p" indicates plasma regime):

$$C_{mp} = p/I = 1.24 \times 10^{-4}[A^{7/16}Z^{-3/8}(Z+1)^{-3/16}(I\lambda\tau^{1/2})^{-1/4}] \quad \text{N-s/J} \tag{9}$$

$$I_{sp\,p} = 652[Z^{3/8}(Z+1)^{3/16}(I\lambda\tau^{1/2})^{1/4}A^{-7/16} \qquad\qquad \text{s} \tag{10}$$

$$T_{ep} = 2980[Z^{3/4}(Z+1)^{-5/8}(I\lambda\tau^{1/2})^{1/2}] \qquad\qquad \text{K} \tag{11}$$

In Eqs. (9)-(11), $Z$ is the average charge state of the plasma plume. This is a number which can be as large as the atomic number of the atoms, depending on $T_{ep}$. $A$ is the average atomic mass; $I$, $\lambda$ and $\tau$ are laser beam intensity (W/m$^2$) on target, wavelength and pulse duration, respectively. $I_{sp}$ is specific impulse, defined earlier.

These are strictly functions of ($I\lambda\tau^{1/2}$) and of $A$ and $Z$. Because of plasma shielding, $A$ and $Z$ are the only parameters that relate to the target material in the plasma regime. Reference 10 shows that despite its simplicity, this model represents data from 47 data sets with various wavelengths, intensities and pulse durations very well. "Bumps" in the

data fitting function are due to changing $Z$. Determining $Z$, which also depends upon $I$ through the Saha equation, can be computationally intensive. In the limits of this theory, $C_m I_{sp}$=0.08, so $\eta_{AB}$=40%. It was unexpected that this theory fits data as well as it does.

## 3.2 Vapor Regime Theory

It is clear that if we can model the vapor regime (left hand side of Figure 3) and if we can find a smooth transition between the two regimes, then we will have the optimum fluence. Vapor regime clearly involves the detailed target properties. It is here that the second temperature $T=T_i$ comes into play in the combined theory.

There are two approaches to modeling the vapor regime. The first uses tabulated pairs of pressure and temperature $(p,T)$ from SESAME tables for some elements[42,52]. By equating laser intensity to energy sinks in the vapor regime, we obtain

$$I = (pv/a)[\gamma/(\gamma-1)][1-T_o/T+q/(C_p T)+(\gamma-1)/2)] + (\sigma\varepsilon/a)T^4 + f(T) \qquad (12)$$

where
$$f(T)=\{\phi(T,x_h)+[x_h\rho_s C_v(T-T_o)]/\tau\}/a \qquad . \qquad (13)$$

In Eq. (12), $a$ is total absorption fraction of the target (not absorption coefficient), $\sigma$ is he Stefan-Boltzmann constant, $\varepsilon$ is emissivity and $\phi$ is a flux limiter from inertial confinement fusion theory. We can relate the quantity $p$ in Eq. (12) to $T$ by using the Riedel equation[57] in conjunction with the SESAME equation-of-state database (e.g., for aluminum) maintained at Los Alamos National Laboratory for $T \leq 7890K$, its triple point.

Eqs. (12) and (13) are wavelength-dependent insofar as $\lambda$ affects the surface absorptivity $a$. Of course, temperature $T$ also affects $a$, so these relationships are recursive. For the infrared to ultraviolet range studied here, we used $0.05 \leq a \leq 0.24$ for modeling aluminum[52].

We now have a numerical solution which relates $p_v$ and $v$ to $I$ over the range corresponding to our $p(T)$ data, and can then compute the vapor regime coupling coefficient as

$$C_{mv} = p_v/I. \qquad (14)$$

A second approach is used where ablation threshold $\Phi_o$ is well-defined but the (p,T) pairs are not available[58]. In this case, where $\xi = \Phi/\Phi_o$, [$\alpha$ (absorption coefficient, m$^{-1}$), is different from $a$ (fraction absorbed)].

$$C_{mv} = [2\rho C^2(\xi-1)\ln\xi/(\alpha\Phi_o\xi^2)]^{1/2} \quad \text{and} \qquad (15)$$

$$I_{spv} = [2\alpha\Phi_o(\xi-1)/(\rho g_o^2\ln\xi)]^{1/2}. \qquad (16)$$

$C$ is a free parameter derived by matching ablated mass density data to the expression

$$\mu=(\rho/\alpha)\ln(C\xi) \qquad \text{kg/m}^2. \qquad (17)$$

11

The $C_{mv}I_{spv}$ product from Eqs. (15) and (16) gives $\eta_{AB}=(g_o/2)C_{mv}I_{spv}=(2C/g_o)(1-1/\xi)$, a function which approaches 1 asymptotically. The coupling coefficient in Eq. (15) maximizes at $\Phi_{opt}=4.2\Phi_o$.

### 3.3 Combined Theory

To make a smooth transition between the vapor and plasma models, we use the ionization fraction $\eta_i$ as a weighting function to combine the two models, attenuating the vapor contribution to zero as ionization becomes complete,

$$C_m = p/I = [(1-\eta_i)p_v + \eta_i\,p_p]/I = (1-\eta_i)\,C_{mv} + \eta_i\,C_{mp}. \qquad (18)$$

Combined theory specific impulse can be obtained in the same way. The combination has yielded good fitting of actual coupling data[52], including the $C_{mopt}$ peak. An example is shown in Figure 5, from Photonic Associates' CLAUSIUS code, an example which shows that real optimum intensities are well represented. Note that $\eta_i \neq Z$.
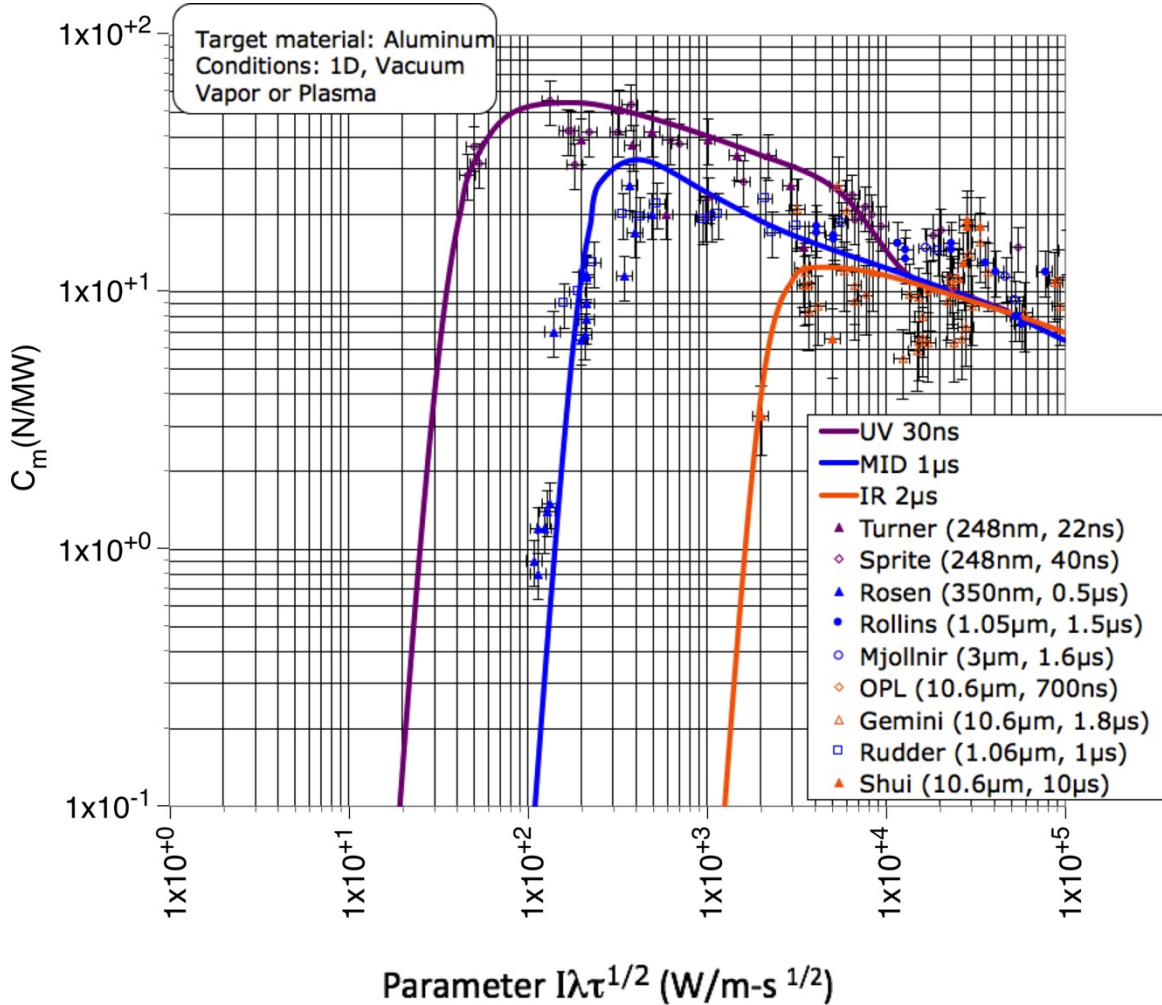


**Figure 5.** Combined Theory. Sources are identified in reference 52.

Efforts[44, 45] to extrapolate $\Phi_{mopt}$ and $C_{mopt}$ across ranges of wavelength and pulse duration, relying on existing simulation results and without doing these calculations, were not successful.

$C_m$, the ratio of impulse to incident laser energy or thrust to power in laser ablation, can be written in several ways -

$$C_m = m_T \delta v_T / W = \delta \mu_E v_E / \Phi = F/P = J/W \qquad (19)$$

with dimensions N-s/J or N/W. We will also quote $C_m$ in units of N/MW, for convenience. In Eq. (19), $m_T$ is target mass, $\delta v_T$ is the change in target velocity, $W$ is pulse energy, $J$ is impulse (N-s), $p$ is surface pressure at the target, $I$ is intensity (W/m²), $\Phi = I\tau$ is fluence on target (J/m²), $v_E$ is exhaust velocity of the laser ablation jet and $\delta \mu_E$ is areal mass density (kg/m²) in the ablation jet column created by one pulse. The change in velocity of the propelled target from a single pulse is

$$\delta v_T = C_m \Phi / \mu_T \qquad (20)$$

and
$$\delta v_{T\parallel} = \eta_c \, \delta v_T \qquad (21)$$

In Eqs. (20) and (21), $\mu_T$ is the target's areal mass density (kg/m²), and $\eta_c$ is an average geometrical efficiency factor taking account of the shape of the target and the fact that the ablation jet will be normal to each facet of its surface, not necessarily antiparallel to the laser beam. The quantity $\delta v_{T\parallel}$ is the change in target velocity parallel to the beam. Eqs. (20)-(21) is a numerically convenient formulation for space applications because we can deliver a fluence $\Phi$ to any object within the illumination diameter having mass density $\mu_T$ and the same $\eta_c$ and be sure that it will gain the same velocity increment from that pulse. Space debris tend to exist in families with similar $\mu_T$. For direct comparison to electric propulsion engines, the thrust to electrical power ratio is

$$C_{me} = \eta_{eo} C_m \qquad (22)$$

Laser electrical-to-optical efficiency $\eta_{eo}$ can range from 25-80%, depending on the laser type. Exhaust velocity can be determined from the product of the easily measured quantities $C_m$ and Q (J/kg ablated) as follows. Where

$$Q = W/\delta m_T = \Phi / \delta \mu_T, \qquad (23)$$

and because $\delta \mu_T = \delta \mu_E$ by mass conservation, it can be seen dimensionally that the product $C_m Q$ is a typical velocity in the ablation jet:

$$v_E = C_m Q. \qquad (24)$$

Ablation thrust efficiency is given by

$$\eta_{AB} = \delta\mu_E v_E^2/(2\Phi) = C_m v_E/2 = C_m I_{sp} g_o/2 \qquad (25)$$

In Eq. (25), $g_o$ is the acceleration of gravity. Eq. (25) makes it clear that $C_m$ and $I_{sp}$ are a constant product in which $I_{sp}$ varies inversely with $C_m$ for engines with the same efficiency. The parameter $Q$ (J/kg ablated) is critical to determining $\eta_{AB}$, which governs the effectiveness of a particular laser and laser ablation fuel. In principle, one may measure $v_E$ with streak photography or Faraday probes to determine $Q = v_E/C_m$, but it is easy to miss a large mass fraction moving at very low velocity (splashing) with this method. Considering the difficulty of measuring ablated material mass with microgram accuracy from before-and-after target mass measurements, the most direct method to determine $Q$ is from

$$Q = \Phi/(\rho_T \delta x) = 2\eta_{AB}/C_m^2 \qquad (26)$$

by measuring the average depth $\delta x$ of the ablation crater with profilometry or a similar technique.

The units of $I_{sp}$ are seconds. Another constant product

$$C_m^2 Q = 2\eta_{AB} , \qquad (27)$$

Defines the ablation efficiency $\eta_{AB}$. Because $\delta\mu_T = \rho_T \delta x$, using Eqs. (19) and (25), the thickness of the target layer ablated in one pulse is

$$\delta x = C_m^2 \Phi/(2\rho_T \eta_{AB}) \qquad (28)$$

For example, with an aluminum target (density $\rho_T = 2700 \text{kg/m}^3$), if $C_m = 30$ N/MW, $\Phi = 30\text{kJ/m}^2$ and $\eta_{AB} = 1$, $\delta x = 5\text{nm}$. At a pulse repetition frequency $f = 50\text{Hz}$, total ablation depth is $\delta x_{tot} = 15\mu\text{m}$ per minute. The ablated surface can be quite uniform, using a beam created with modern methods of apodization.

## 3.4 Optima

For each mission, there is a different kind of optimum from the $C_{mopt}$ giving maximum mechanical coupling. This optimum, $C_{mopt-MS}$, gives minimum energy cost to complete the mission. For example, for one Earth to LEO mission simulation, $C_{mopt-MS}$ was 200-500 N/MW[59] [Figure 6]. In the figure, we see that in this simulation $C_m = 1000$N/MW has an infinite cost for a 200s flight (dot at the top). Yet another $C_m$ optimum is the one that delivers the highest mass ratio $m/M$ to orbit for LEO launch. This choice corresponds to choosing maximum $I_{sp}$ and also to increased laser power for flights opposing gravity or those which require rapid acceleration.
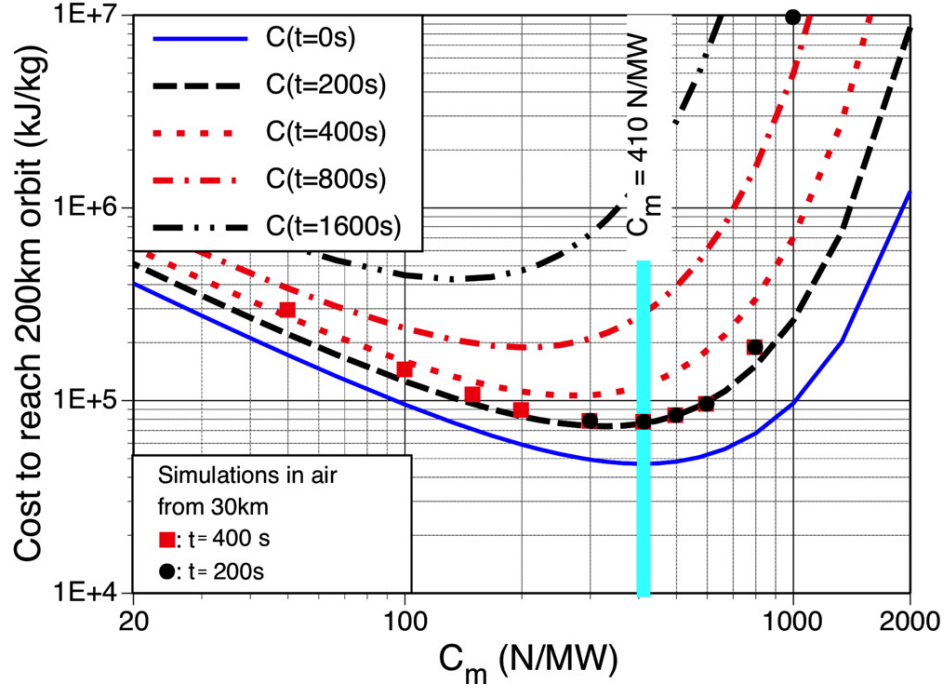
**Figure 6.** Each mission has an optimum mission cost impulse coupling coefficient. In this case, a 1MW average power laser launch from 35km to LEO, $C_{mopt-MS}$ is 300-500N/MW for a 200s flight. Lines are theory, dots are simulations for a real atmosphere [adapted from ref. 43]. Optima depend on laser power.

## 4.0 Experiments
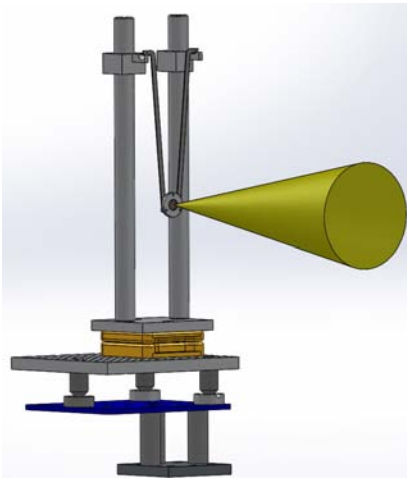
## 4.1 Impulse Pendulum Measurements



**Figure 7.** LULI pendulum. The cone indicates the laser beam.

In order to determine $C_m$, we need laser energy $W$ on target and impulse $J$ delivered to it. $J$ can be measured using deflection of a pendulum,

$$J = m_{eff}\{2g_oL[(1 - \cos(\beta/2)]\}^{1/2}. \qquad (29)$$

In Eq. (29), $L$ is the distance from the pendulum fulcrum to the point where laser impulse is generated. $\beta$ is the maximum deflection angle of a probe beam reflected from a mirror attached to the pendulum, twice the pendulum deflection angle $\theta$. The period of a pendulum depends only on $g_o$ and $L$, not on the mass, so that cannot be used to get impulse $J$.

One can also use the powerful "PDV" twin-laser technique [see laser velocimetry section], to get velocity directly. We used both in this measurement

15

series. In either case the effective mass $m_{eff}$ of the target-plus-pendulum must be known.

$$m_{eff} = \Sigma_i (m_i L_i)/L \qquad (30)$$

Because zero mass pendula don't exist, $m_{eff}$ is a crucial parameter determining impulse from pendulum measurements. For us, with a 0.0191kg pendulum assembly (Figure 7) and a 0.0038 kg target mounted, the effective mass was 0.0153kg, about 80% of the pendulum assembly total mass of 0.01909. $L$ was 0.0148m.

## 4.2 Laser Velocimetry

Laser velocimetry is one of the principal diagnostics for shock physics experiments. Historically, two methods have been traditionally used for measuring velocities in the km/s range, the VISAR system (Velocity Interferometer System for Any Reflector)[60] and the Fabry-Pérot system[61]. A new method called PDV (Photonic Doppler Velocimetry) based on heterodyne detection is now used to measure the velocity of the matter under shock or of a flying object[62,63]. This method may be used with one or two lasers. For our application, we use only one laser, due to the problem of laser coherences of the two different lasers for very low velocities and associated high time recording. We used an adaptation of the classical PDV diagnostic (Figure 8) with two methods to deduce the velocity or displacement curves [ref. 64]. For the classical PDV
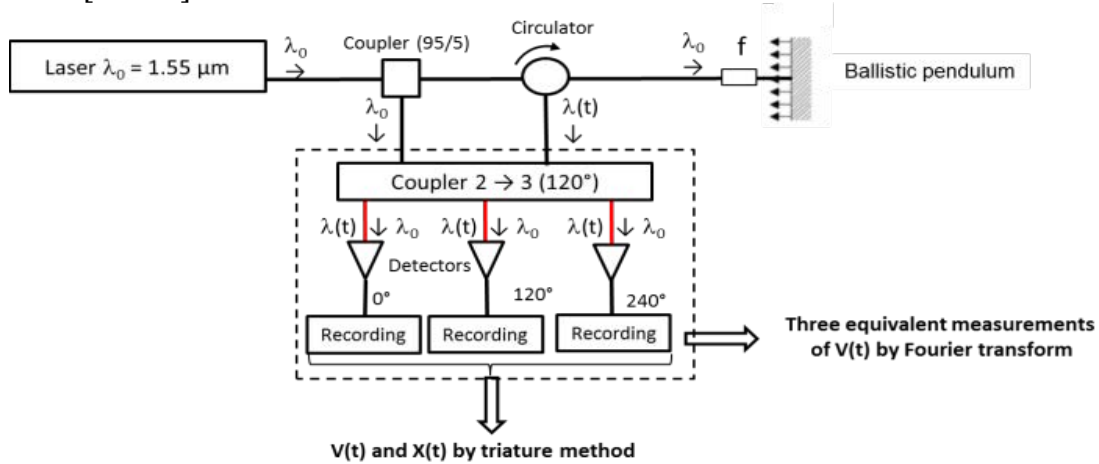


**Figure 8.** The experimental setup used to measure the pendulum velocity curve

system, we deduce the $v(t)$ curve by a Fourier transform method without velocity sign. With the triature method IDF (Interférométrie de Déplacement Fibrée), we may deduce the $v(t)$ curve with its associated sign from an analytical formula applied on the three PDV signals. An example of experimental result is given in Figure 9.

**Table III.** Elfie Laser Parameters

| Wavelength | 1057nm | |
|---|---|---|
| Pulse duration | 400 fs | 80 ps |
| Pulse energy (J) | 12 | 12 |
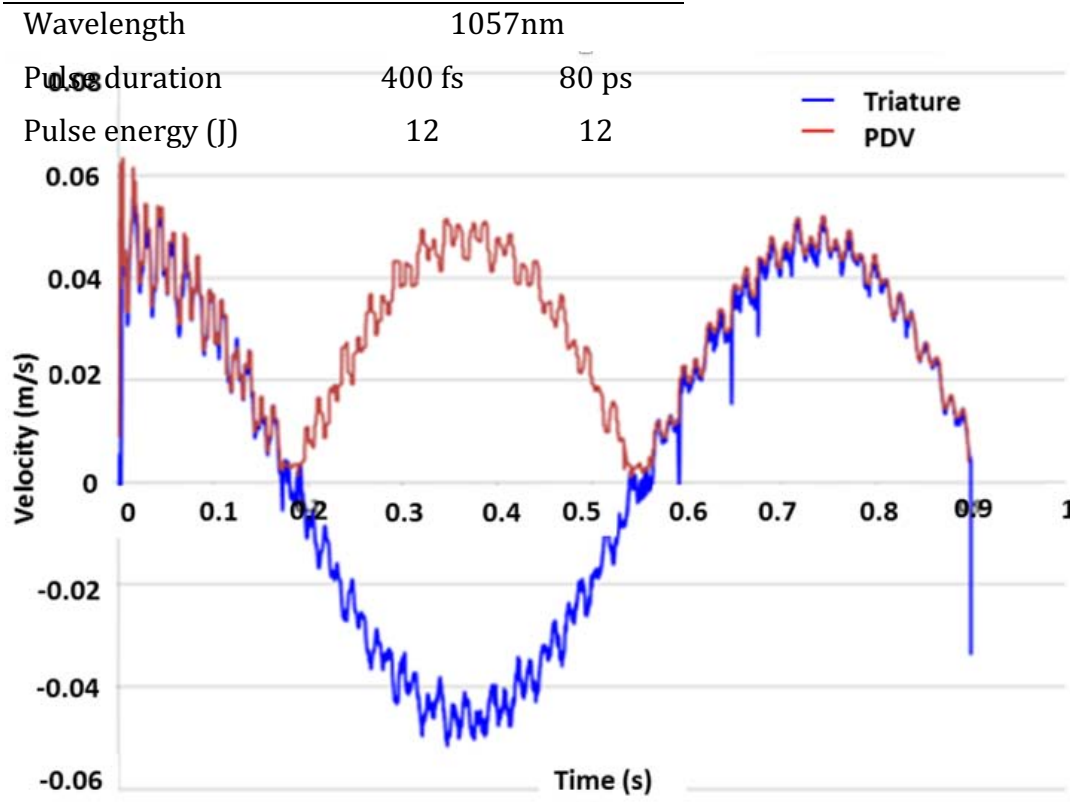


**Figure 9.** $v(t)$ curves deduced from PDV (red) and IDF (blue) on shot 48 on POM target]

## 4.3 Laser

The "Elfie" laser at LULI, the Laboratoire pour l'Utilisation des Lasers Intenses at École Polytechnique, uses the CPA technique and can operate at 1057 nm (1ω) as well as 528nm (2ω) (Table III). At 1ω, energy ranges up to 12 J on target with a repetition interval of 20 min. The contrast ratio (ratio between pulse and prepulse intensity) is better than $10^7$. At 2ω and 400fs, the ELFIE laser offers 5J pulse energy. It also offers the possibility to modulate the pulse duration from 400fs up to 80 ps by changing parameters of the compressor. The experimental setup is shown in Figure 10.
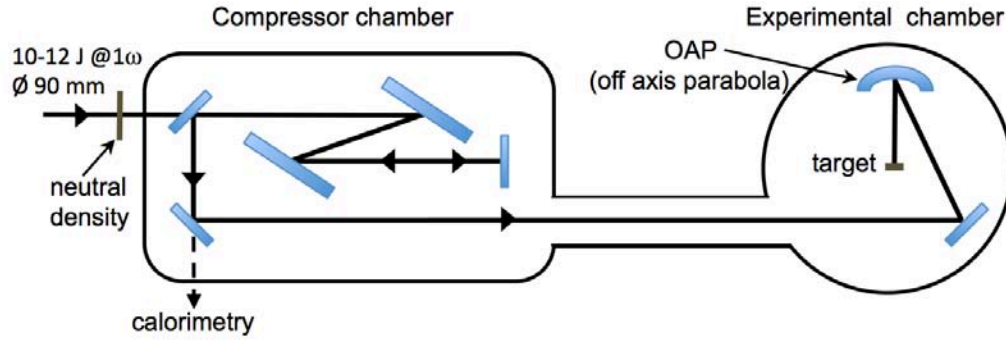
**Figure 10.** LULI/Elfie experimental layout

## Practical Matters

In ten days of actual operation for this two-week program, we accumulated 64 shots, about 6/day, limited by the time required to mount a new target, align diagnostics, and to pump down the target chamber for each shot. Statistics on results from such a few shots on many materials are not worthwhile.

We used calibrated neutral density filters to adjust energy on target. Beam diameters on target were 3.0 and 6.9mm with an extremely uniform laser ablation spot on target. Pressure was less than 0.1 torr for all shots. Figure 11 illustrates the illumination uniformity.

## 4.4 Target Materials

We chose POM as a target material out of curiosity, because Myrabo[48] found it to be a high-thrust material for his "Lightcraft" at 10.6μm wavelength, and we wanted to see if that advantage was transferred to 1.06μm.



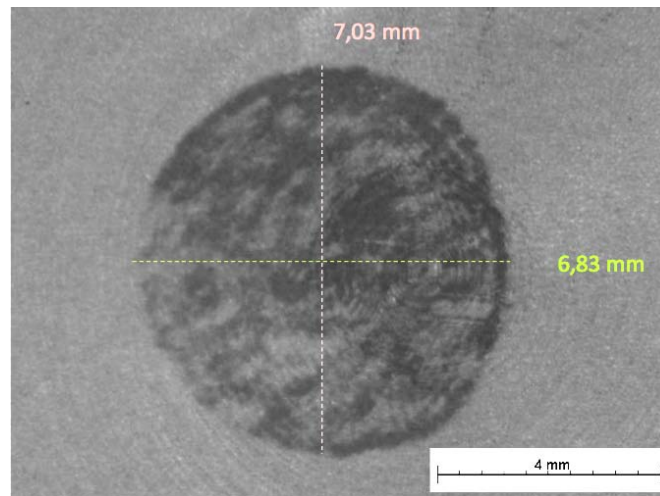**Figure 11.** 0.377cm$^2$ target illumination spot. Photo of Delrin (POM) target after metallization with 7nm Pt

We chose Al because it is a major spacecraft component and this work is applicable to propelling objects in space. W and Au were chosen for comparison with ref. 25 results. Ta was chosen to give a further idea of the variation of $C_m$ with atomic weight.

## 5.0 Results

## 5.1 Momentum Coupling Coefficient

Figures 12-15 show the $C_m$ values we obtained vs. incident fluence $\Phi$. For POM and Al in this short-pulse regime, these are the first measurements in the literature that give a reasonably clear value for the fluence $\Phi_{opt}$ at which maximum $C_m$ occurs. A word about how we identified "optimum," and its uncertainty, from our data. Where we had enough data to show a clear trend, we chose the fluence at which $C_m$ was a maximum, or one at which more fluence could not produce a better result for $C_m$.
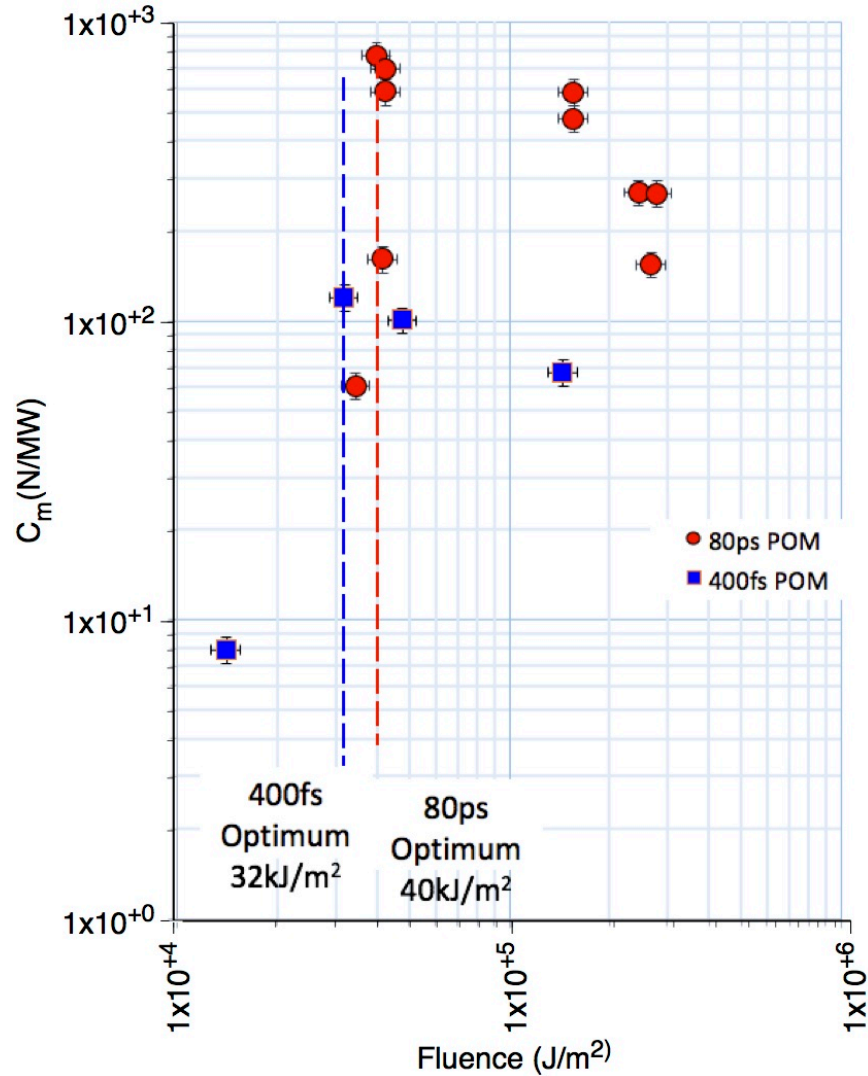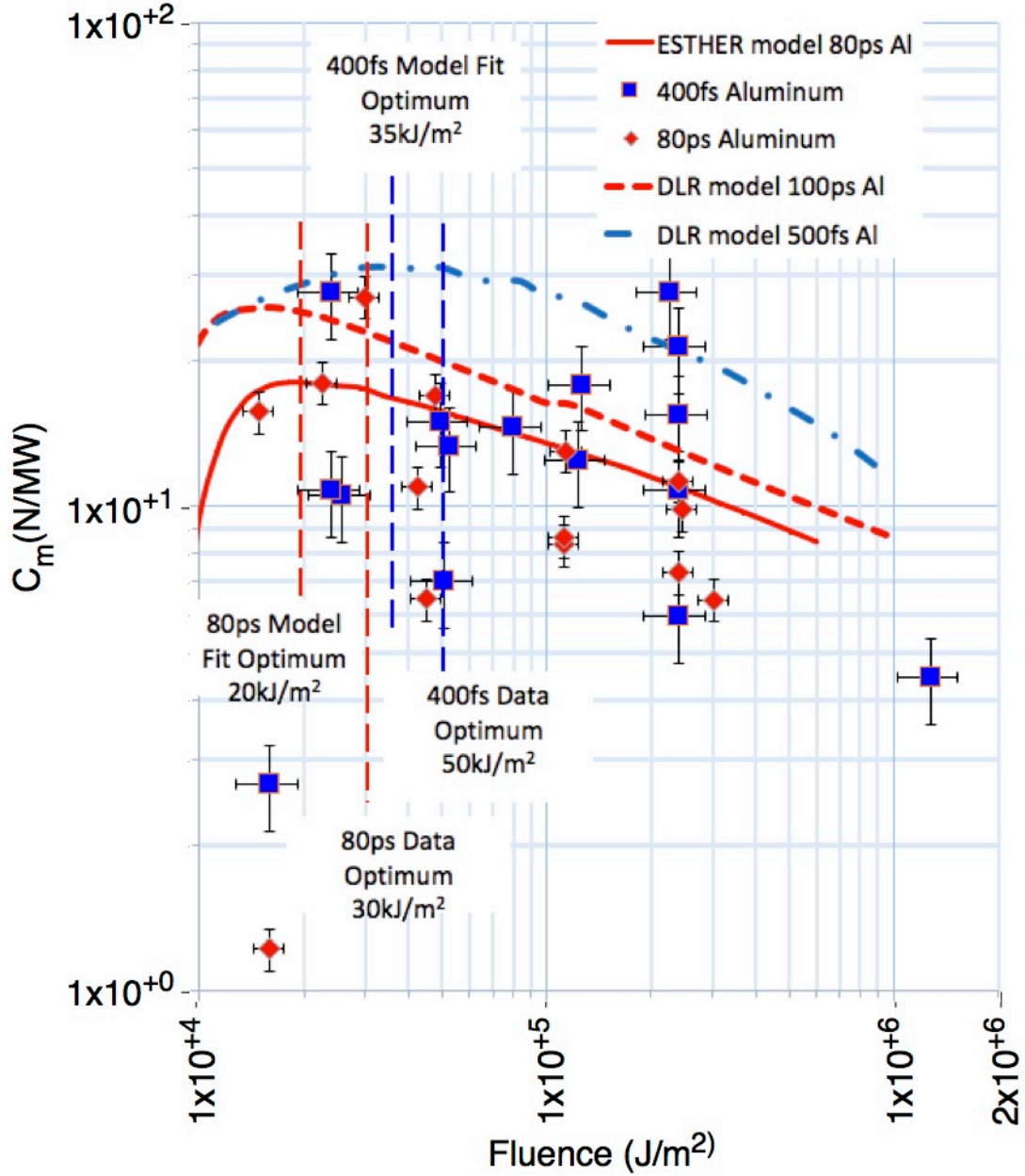


**Figure 12.** $C_m$ for POM at 80ps and 400fs, 1057nm

19

**Figure 13.** $C_m$ for aluminum at 100ps and 400fs, 1057 nm. Experimental data compared with simulation results. For the 80ps data, $\Phi_{opt}$ is 30kJ/m². For 400fs, we chose $\Phi_{opt}$ = 50kJ/m² because, as a practical matter,  nothing is gained by going to higher fluence. The solid line shows a preliminary modeling using the CEA ESTHER code at 80ps. The dashed lines show simulation results from DLR with Polly-2T for 100ps and 500fs pulse durations at 1064nm (see §5.1 for description of these codes).

In general, our error bars for an individual data point are ±10% for both fluence and $C_m$. The uncertainty in $C_m$ may have been due to differences in sample preparation. The uncertainty of $\Phi_{opt}$, particularly where the data shows a steep rise or fall in $C_m$ on either side of $\Phi_{opt}$ is also shown in the table. This uncertainty has less meaning in
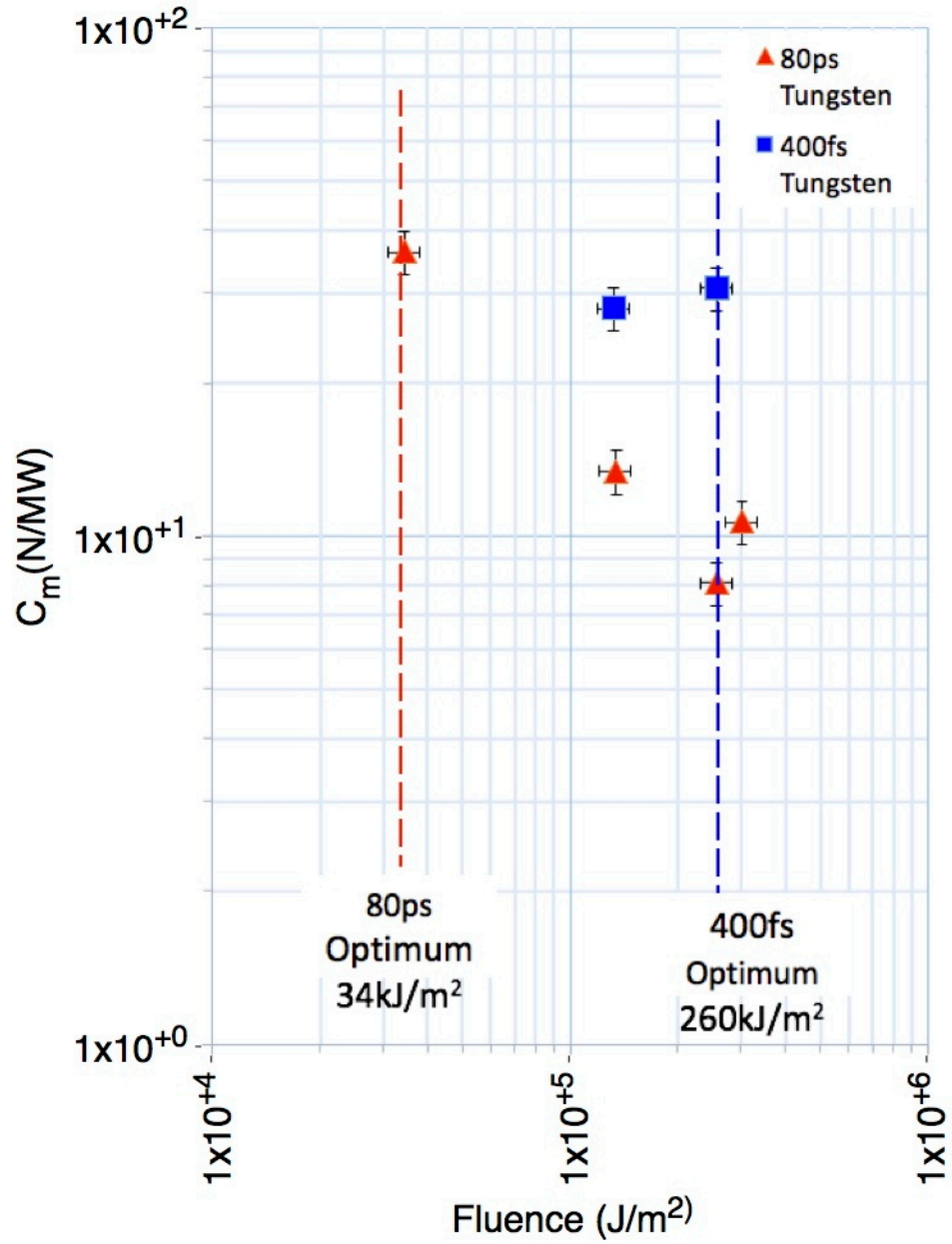
cases where we had few data [Figures 14 and 15].



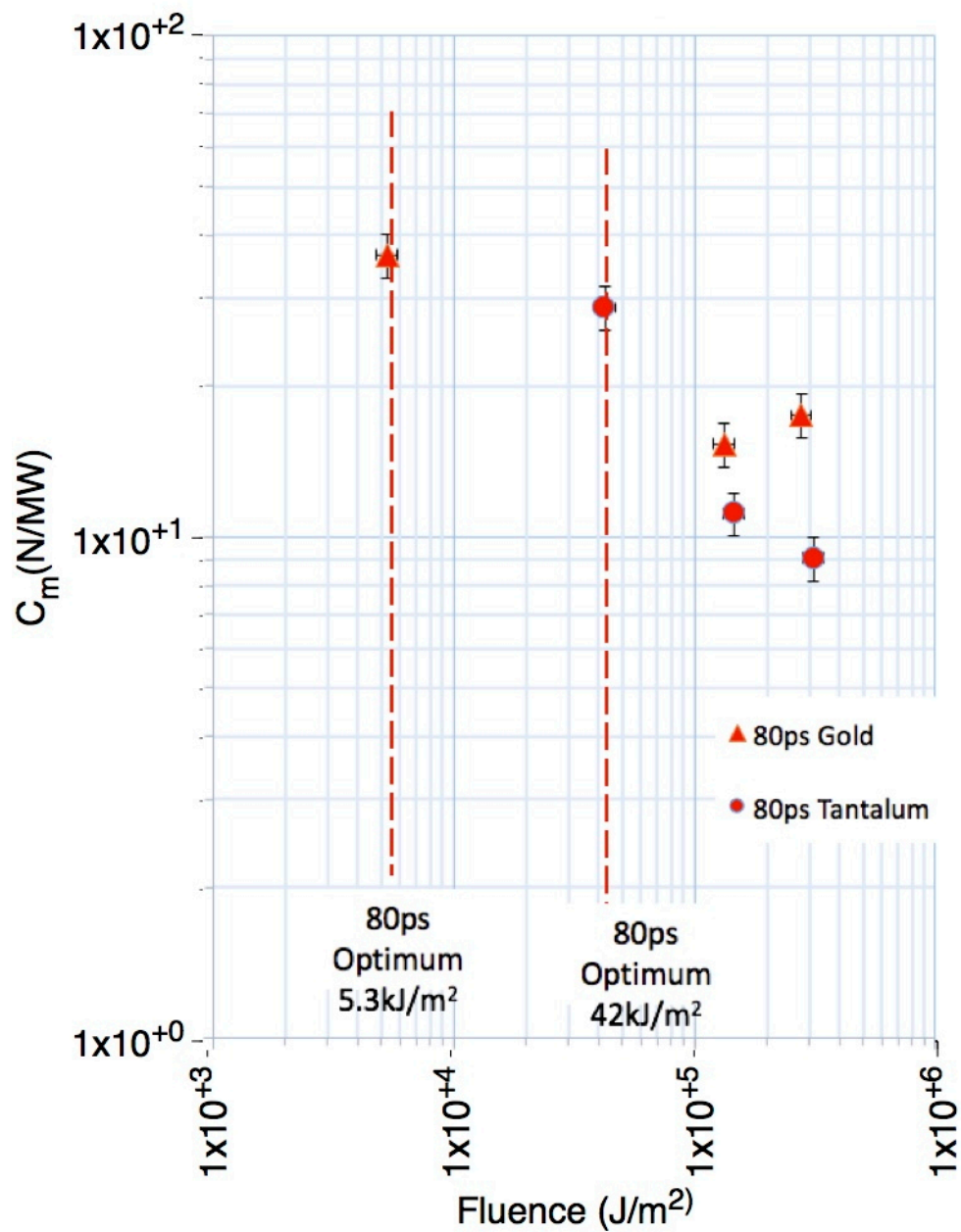**Figure 14.** $C_m$ for W at 80ps and 400fs, 1057 nm.

**Figure 15.** $C_m$ for Au and Ta at 80ps, 1057 nm

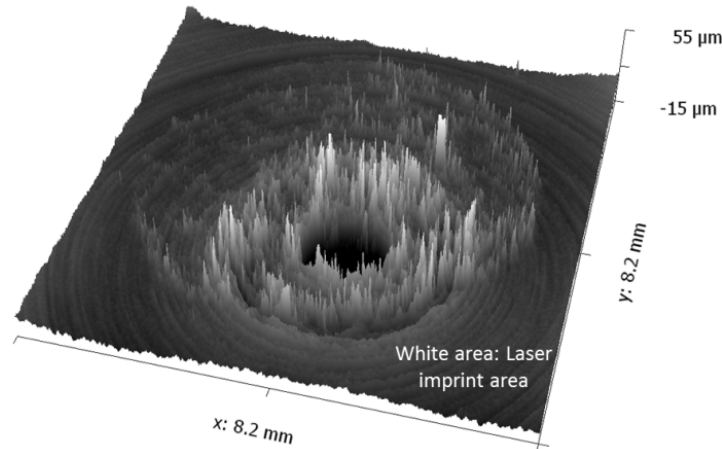Our aluminum targets were 99.9% pure, from Goodfellow, Inc.



**Figure 16.** 3D representation of the altitude profile on Delrin. Most of the structure we see arises from machining defects.

ESTHER[64] is a Lagrangian monodimensional hydrodynamic code which includes the resolution of the Helmholtz equation which allows us to describe the laser propagation and absorption into the matter. We use a multi-phase equation of state for aluminum. Optical absorption is calculated by using Palik data[65] when the matter is solid. In the plasma domain, absorption is given by classical inverse Bremsstrahlung formula[66]. For aluminum, we also could use hydrodynamic simulations with the code Polly-2T, described in more detail in Povarnitsyn, et al[67], to model the two pulse durations. This code is based on the two-temperature model for laser-mater interaction with metal targets[68], and uses the Helmholtz equation[69] for coupling laser energy into the target. Semi-empirical equations of state are taken for material description including a dynamic model for dielectric permittivity, electron-phonon coupling and heat conductivity for a wide range of temperatures. Polly-2T was provided by Mikhail Povarnitsyn from the Joint Institute of High Temperatures at the Russian Academy of Sciences, Moscow.

## 5.2 Ablated Mass Measurements

Tests with both confocal chromatic analysis (CCA, STIL sensor) and scanning electron microscopy analysis (SEM, FEI XL30 ESEM LaB6) were inconclusive regarding ablated mass. The samples were too rough and irregular to permit deduction of ablation depth in the the laser illuminated regions. [Figures 16-18]
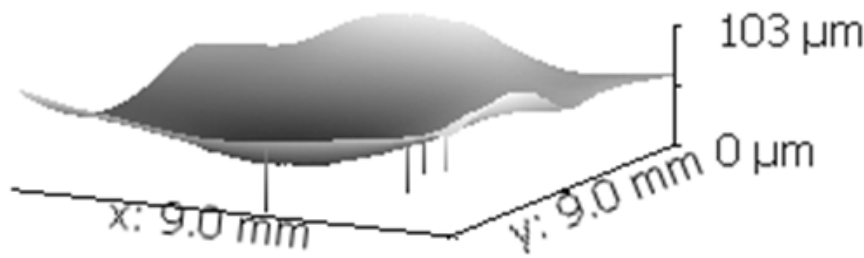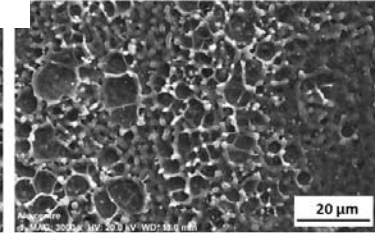
of at most 770μm for POM
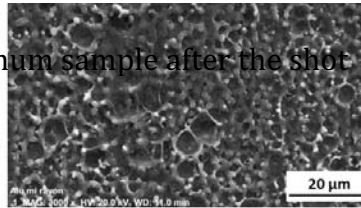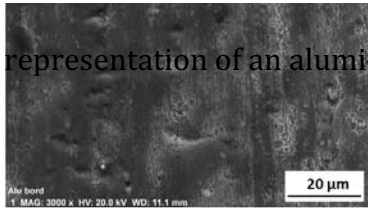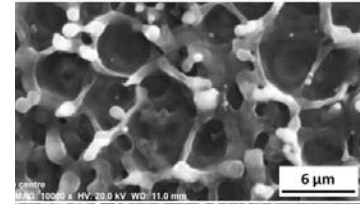ximum values of $C_m$ and $\Phi$
ising.

**igure 18.** (a) 3D representation of an aluminum sample after the shot

**Figure 17.** SEM image of an aluminum sample with magnifications 10k(top) and 3k(bottom) at $\Phi$ =10kJ/m². Left-to-right : unilluminated sample, middle, and center of illumination. We see characteristic structure of short pulse illumination, but no clear boundary that permits estimation of depth. As regards ablation depth, similar results were obtained with tungsten and tantalum samples, and with SEM of Delrin which we metalized with platinum after the shot to make SEM possible.

**Table IV.** Optimum coupling results for Al and POM at 1057nm

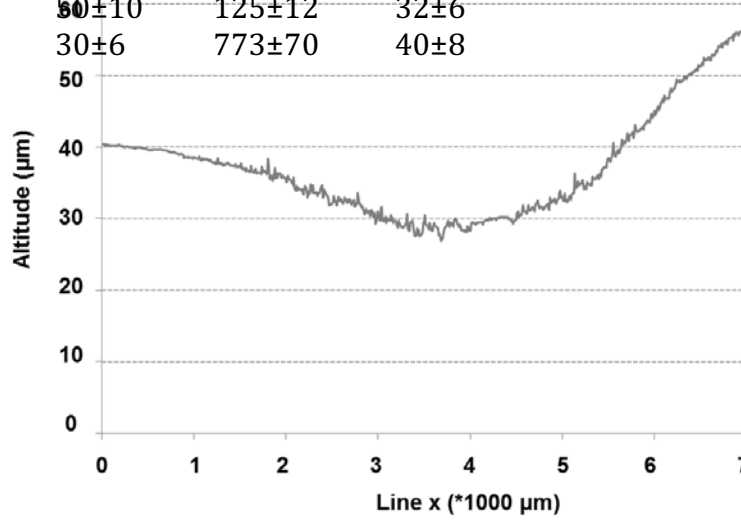| Material | Al | | POM | |
|---|---|---|---|---|
| | $C_m$(N/MW) | $\Phi$(kJ/m²) | $C_m$(N/MW) | $\Phi$(kJ/m²) |
| Pulsewidth | | | | |
| 400fs | 30±5 | 50±10 | 125±12 | 32±6 |
| 80ps | 28±5 | 30±6 | 773±70 | 40±8 |



**Figure 18** (b). Altitude profile of a sample, using CCA. Our measurements gave an inconclusive result for ablation depth.

Table IV gives our results for Al and POM, with their uncertainties.

## 6.0 Discussion

Our best estimates of measurement uncertainty are incorporated into the error bars shown in Figures 12-15. Error bars for $C_m$ and $\Phi_{opt}$ data for Al at 400fs are ±20% rather than ±10% in other data. This may be partly due to energy uncertainty early in the 10-day experiment series when the 400fs data were taken.

Modeling shown in Figure 13 indicates slightly higher $C_m$ for Al at 400fs than at 80ps. Data shows a similar trend although scatter makes conclusions tenuous. Both data and modeling show higher $\Phi_{opt}$ data for Al at 400fs than at 80ps.

We find similar $C_m$ values among the metals, and not much difference from previous work in the ultrashort range, nor from the DLR simulation[27,70] for the longer pulses. For POM, we found a gigantic $C_m$ but there is no obvious reason why it should be large at both 1.06 and 10.6µm wavelengths other than its large molecular mass. As to why it should give a factor-of-six smaller result at 400fs than at 80ps, ultrashort-pulse $C_m$ should depend primarily on tensile strength, lower $\sigma_y$ giving higher $C_m$. We do see that effect comparing $C_m$ for POM to that for Al in the 400fs data [Table V].

For aluminum, the measured coupling coefficient at 80ps is about three times

smaller than the 100N/MW we have assumed at 100ps for some proposed systems based on LASNEX simulations in ref. 26. This reference treated 530nm and 20ps, while our applications were for 355nm and 80ps. Still, this discrepancy is significant. The optimum fluence is four times larger than we assumed previously.

These results are not a severe limitation because higher fluence offsets lower $C_m$ to give the same performance originally claimed for these systems,[44,45] albeit at the cost of higher laser average power.

### TABLE V: New Results Compared to Existing Short Pulse C_m Data

| Fluence (kJ/m$^2$) | $C_{mopt}$ (N/MW) | Pulsewidth | Material | Reference no. |
|---|---|---|---|---|
| 20 | 18 | 50fs | Ti | 23 |
| 5.2 | 42 | 130fs | Mo | 24 |
| 20 | 40 | 130fs | W | 25 |
| 17 | 85 | 130fs | Au | 25 |
| 10 | 25 | 130fs | Li | 25 |
| 13 | 49 | 130fs | Fe | 25 |
| 13 | 25 | 130fs | GAP | 25 |
| 12 | 18 | 130fs | Al | 25 |
| 30±20% | 30±20% | 400fs | Al | This work |
| 32±10% | 120±10% | 400fs | POM | This work |
| 260±10% | 30±10% | 400fs | W | This work |
| 5.3±10% | 37±10% | 80ps | Au | This work |
| 42±10% | 29±10% | 80ps | Ta | This work |
| 40±10% | 780±10% | 80ps | POM | This work |
| 30±20% | 28±20% | 80ps | Al | This work |
| 36±10% | 36±10% | 80ps | W | This work |

On the good side, Eq. (4) shows that when we do deliver the larger 80ps fluence with much lower $C_m$, we may expect an aluminum surface to have about twice longer lifetime per laser pulse under optimum irradiation conditions.

Our most pleasant surprise was the performance of POM, which gave an 80ps $C_m$ value of 773N/MW, larger than any other reported unconfined, passive (nonenergetic) material at short pulse durations.

This $C_m$ is too large for most laser launch projects [see Figure 6], *but* it is useful from the following point of view: for laser launch projects, using the Table II parameters, we predict that we can cast ablation fuel from a mixture of, e.g., Al dust and POM to obtain 300N/MW, or any other value we want in the range from 30 to 770 at 80ps. The required fluence (~30kJ/m$^2$) is about the same for both materials. For reasons

having to do with the absence of available laser system designs at 400fs capable of 100 to 1kJ pulses, this pulse duration is presently not attractive compared to 80ps, so it doesn't concern us that $C_{mopt}$ for POM at 400fs is much less than at 80ps. We can also easily create a fuel with $C_m$=100N/MW, as required for the reference 44 and 45 space system designs. We do expect larger $C_m$ for metal targets at the second and third harmonics (530 and 352nm).
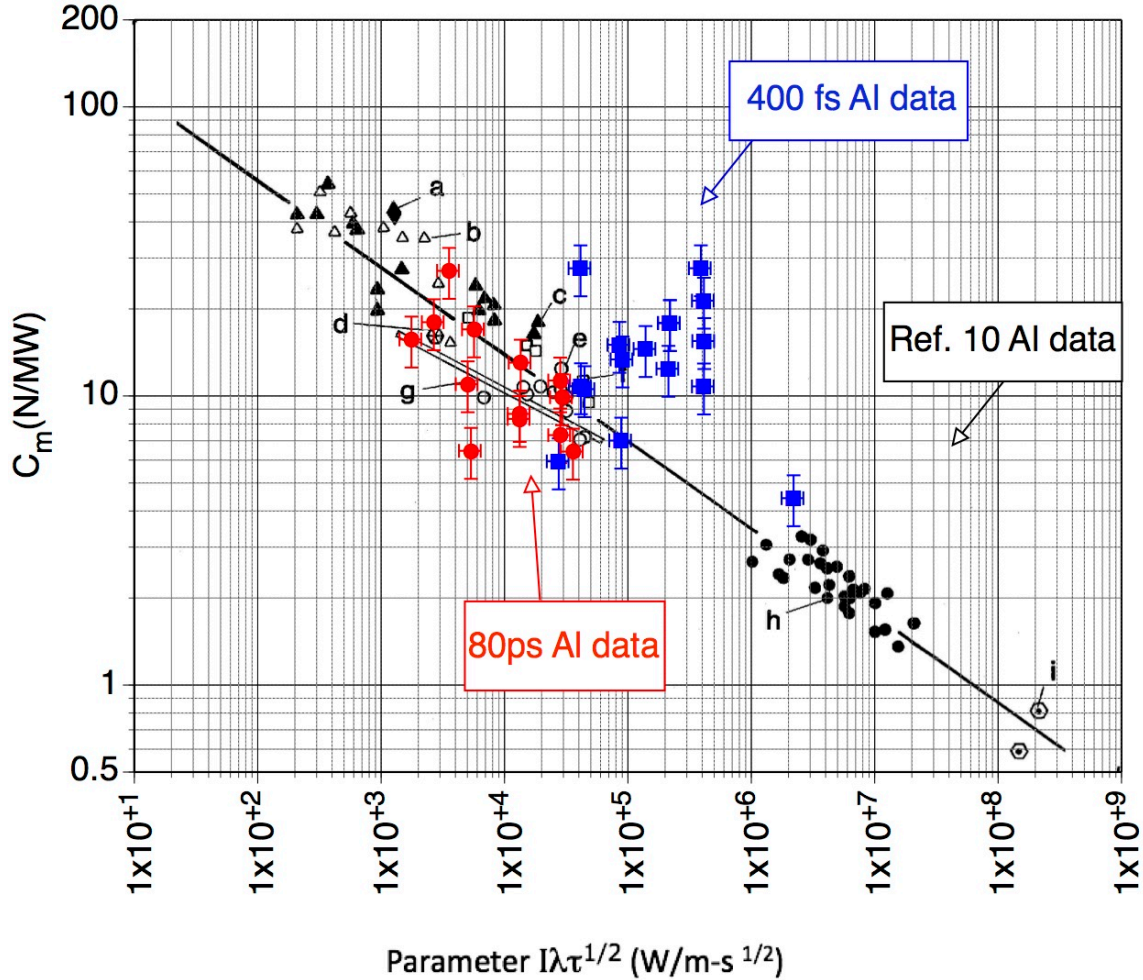


**Figure 19.** Our data vs. plasma theory from ref. 10 and data listed there (grey). The horizontal axis parameter is explained in §3.

Figure 19 show how our $C_{mopt}$ data for aluminum compares with that of other authors at 80ps and 400fs. Clearly there is good agreement at 80ps, and less agreement at 400fs as expected following the §1.4 discussion.

At 400fs, it is reasonable for Au and Fe to have higher $C_m$ because of their larger atomic weight. At 80ps, Au and W have larger $C_m$ than Al and Ta for the same reason. The limited number of data points for these materials did not permit strong conclusions. As we pointed out earlier, the major influence at 50-400fs should be a dependence on tensile strength, rather than atomic weight, lower $\sigma_y$ giving higher $C_m$. This prediction is approximately borne out. POM performs dramatically at 80ps.
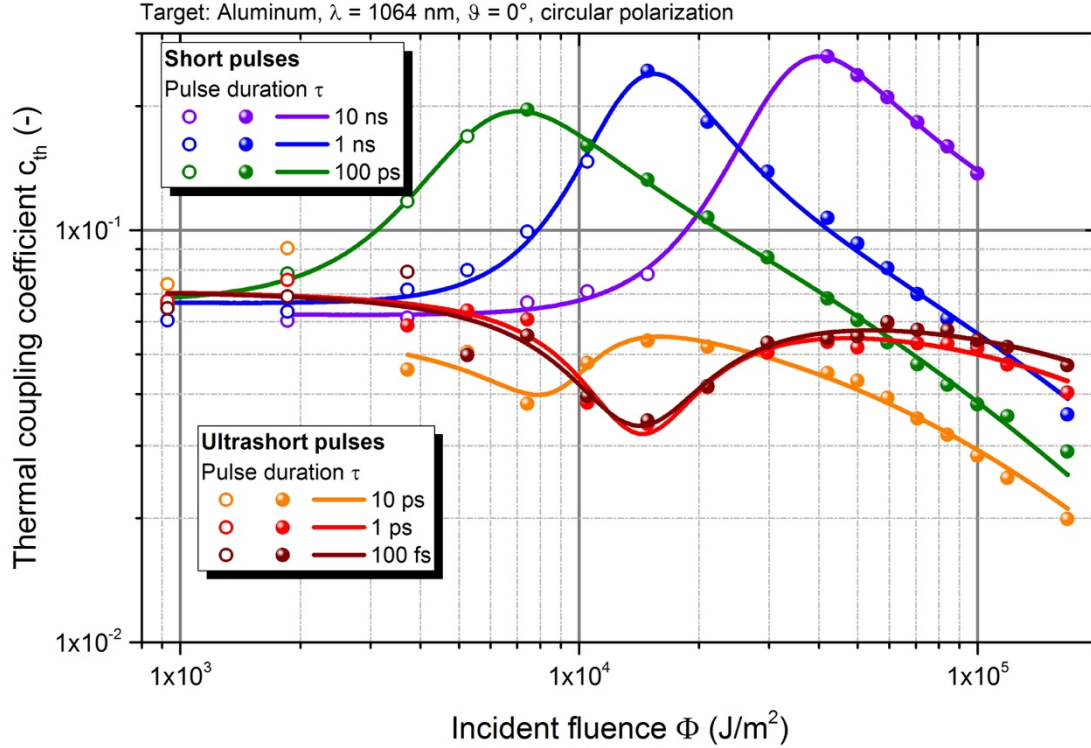
**Figure 20.** Numerical simulation of thermal coupling vs. pulse duration and laser fluence on aluminum, including shock thermalization. Full symbols denote ablation whereas hollow symbols show thermal coupling below ablation threshold.

## 7.0 Conclusions

For the first time, we have measured the single-pulse mechanical coupling coefficient to POM and some metals at 1057nm, 80ps and 400fs, and the associated optimum fluences. We found giant $C_m$ results for POM at 80ps, 1057nm. For Al, there was not much difference from previous work in the ultrashort range, nor from Scharring's simulation for the longer pulses. We found a large difference from Fournier's simulation for Al using LASNEX, on which we based some of our past laser propulsion performance extrapolations. We can compensate these by using more laser fluence. We were not able to measure mass loss in this series. We proposed using a cast mixture of Al dust and POM in varying proportions to obtain $C_m$ values between 30 to 770N/MW. We intend to buttress this proposal with measurements in the near future.

## 8.0 What is Still Unknown

Two measurements are still urgently needed: the ablation efficiency and thermal coupling coefficients associated with our data. Figure 20 shows an analysis of simulations in reference 70 with respect to the residual heat remaining in the target after ablation. The results shown for ultrashort pulses, typically known as "cold ablation," give us hope for the utility of 1-10ps pulses. These should demonstrate $C_{th}$<6% at ~30kJ/m². However, at fluences above 6kJ/m², 10-100ps pulses are the best from this crucial viewpoint. Such fluences will be useful when maximum $I_{sp}$ rather than maximum $C_m$ is the goal (see §3.4). This effect arises because the longer pulses do not add so much thermal coupling from shock.

## 9.0 Acknowledgment

## 10.0 References

[1] F. Tsander, "Flight to other planets," (1924) in Ye. Moshkin, *Development of Russian Rocket Technology*, Mashinostroyeniye Press, Moscow (1973) (in Russian)

[2] K. Tsiolkovsky, "Plan of Space Exploration," (1926) (in Russian), available in English in "Exploration of the Universe with Reaction Machines: Exploring the Unknown," NASA History Series. NASA SP 4407, Washington, D.C. (1995)

[3] H. Oberth, "Die Rakete zu den Planetenräumen", (The Rocket to the Planet Spaces) Oldenbourg Verlag, München (1923)

[4] E. Sänger, "Zur Theorie der Photonenraketen," Probleme der Weltraumforschung (IV. Internationaler Astronautischer Kongress, Zürich 1953; S. 32, Biel-Bienne: Laubscher (1955)

[5] A. Kantrowitz, "Propulsion to Orbit by Ground-Based Lasers," *Astronautics and Aeronautics*, **10**, No. 5, 1972, pp. 74–76.

[6] C. R. Phipps, "Pulsed lasers for clearing debris in LEO and GEO," paper LSSE1-1, *Optics and Photonics International Conference*, Yokohama, 17-20 May 2016 (2016)

[7] Yu. Afanas'ev, N. Basov, O. Krokhin, N. Morachevskii and G. Sklizkov ,"Gas-dynamic process in irradiation of solids", *Soviet. Physics. -Technical. Physics.* **14**, no. 5, 669-676 (1969)

[8] A. Augustoni, P. Ermer, R. Heckler, G. Kuwashima, J. McKay and R. Rudder,"The interaction  of high energy single pulse XeF laser radiation with solid targets," report AFWL-TR-85-126, 1986, U.S.Air Force Research Laboratory,  AFB, NM (not paginated)

[9] P. Combis, J. David and G. Nierat, "Mesure des Effets Mécaniques dans les Expériences d'Interaction Laser-Matiere a Eclairement Modéré", *Revue Scientifique et Technique de la Defense, CEL-Valenton no.4* 1992,pp. 59-75, Centre des Etudes Limeil-Valenton, B.P. no. 27, 941956 Villeneuve-Saint-Georges Cedex, France

[10] C. Phipps, T. Turner, R. Harrison, G. York, W. Osborne, G. Andersson, X. Corlis, L. Haynes, H. Steele, K. Spicochi and T. King, "Impulse Coupling to Targets in Vacuum by KrF, HF and $CO_2$ Lasers" *J. Appl. Phys.* **64** , pp. 1083-96 (1988)

[11] C. Duzy, J. Woodroffe, J. Hsia and A. Ballantyne, "Interaction  of a pulsed XeF laser with an aluminum surface", *Applied. Physics. Letters.* Vol. **37**, no. 6, 1980, pp. 542-544

[12] J. McKay and P. Laufer, "Survey of Laser-Produced Pressure and Impulse Data," Physical Sciences, Inc., Final Rept. PSI-1012/TR-757, New England Business Center, Andover MA, 1987, pp. 1–236.

[13] D. Gregg and S. Thomas, "Momentum transfer produced by focused laser giant pulses", *Journal of. Appied Physics.* Vol. **37** no.7., 2787-2789 (1966)

[14] B. Xu, Q. Wang. X. Zhang, S. Zhao, Y. Xia, L. Mei, X. Wang and G. Wang, " "Impulse transfer to the surface of aluminum and copper from a pulsed Nd:YAG laser," *Appl. Phys.* **B 57** 277-80 (1993)

[15] D. Rosen, D. Hastings and G. Weyl, "Coupling of pulsed 0.35-mm laser radiation to titanium alloys", *Journal of. Applied. Physics.* Vol. **53** no. 8  pp. 5882-5890 (1982 )

[16] D. Rosen, P. Nebolsine, and P. Wu, "Laser impulse applications research", paper V1, *Proceedings of the. AIAA Conference on the Dynamics of High Power Lasers, Cambridge, MA* (1978)

[17] R. Rudder, report AFWL-TR-74-100, U. S. Air Force Research  Laboratory, Kirtland Air Force Base, NM, pp. 189-198 (1974)

[18] V. Shui, L. Young and J. Reilly, "Impulse transfer from pulsed $CO_2$ laser irradiation at reduced ambient pressures", *AIAA Journal* vol. **16,** 649-50 (1978)

[19] I. Ursu, I. Apostol, D. Barbulescu, I. Mihailescu and M. Moldovan, "Plasma-target coupling in the case of TEA-$CO_2$ laser produced breakdown in front of a solid target", Optics Communications..vol. **39**, 180-185 (1981)

[20] T. Pucik and R. Crawford, "Optical Laser Impulse Coupling Data Package", RDA report 2.28.90. 1990,  Logicon/R&D Associates, P.O.Box 92500, Los Angeles, CA 90009, not paginated

[21] B. D'Souza, "Development of impulse measurement techniques for the investigation of transient force due to laser-induced ablation," Ph. D. dissertation (2007)

[22] B. Wang, H. Tsuruta and A. Sasoh, "Impulse generation by multiple-pulse laser ablation with oblique incidence," paper LSSE2-4, *Proc. Laser Solutions for Space and the Earth May 17-20, 2016*, Yokohama (2016)

[23] E. Loktionov, Yu. S. Protasov and Yu. Yu. Protasov, "Thermophysical and gas-dynamic characteristics of laser-induced gas-plasma flows under femtosecond laser ablation," *Quantum Electronics*, **44**, 225-232 (2014)

[24] C. Phipps, J. Luke, D. Funk, D. Moore, J. Glownia and T.Lippert, "Measurements of laser impulse coupling at 130fs", **SPIE 5448**, pp. 1201-1209 (2004)

[25] C. Phipps, J. Luke, D. Funk, D. Moore, J. Glownia and T. Lippert, "Laser Impulse Coupling at 130fs," *App. Surf. Sci..*, **252** 4838-4844 (2006)

[26] K. Fournier, "LASNEX calculations of laser-coupling coefficients for Al targets," UCRL-Pres-226849, p.29 (2006)

[27] S. Scharring, J. Wilken and H.-A. Eckel, "Laser-based removal of irregularly shaped space debris," *Optical Engineering*, **56**, p.011007-4 (2017). doi:10.1117/1.OE.56.1.011007

[28] C. R. Phipps, M. Birkan, W. Bohn, H.-A. Eckel, H. Horisawa, T. Lippert, M. Michaelis, Y. Rezunkov, A. Sasoh, W. Schall, S. Scharring and J. Sinko, "Review: Laser Ablation Propulsion," *J. Propulsion and Power*, **26** no. 4 pp. 609-637 (2010)

[29] C. Phipps, unpublished

[30] A. Ovsianikov, S. Passinger, R. Houbertz and B. Chichkov, *Laser Ablation and Its Applications*, Springer, New York, 2007, pp. 121– 156, Chap. 6

[31] B. Esmiller, C. Jacquelard, H.-A. Eckel and E. Wnuk, "Space debris removal by ground-based lasers: main conclusions of the European project CLEANSPACE," *Appl. Opt.* **53**(31): I45 – I54 (2014), figure used by Dr. Eckel's permission

[32] R. Soulard, M. Quinn, T. Tajima and G. Mourou, "ICAN: a novel laser architecture for space debris removal," *Acta Astronaut.* **105** (1) 192–200 (2014)

[33] T. Ebisuzaki, M. Quinn, S. Wada, L. Piotrowski, Y. Takizawa, M. Casolino, M. Bertaina, P. Gorodetzky, E. Parizot,T. Tajima, R. Soulard and G. Mourou, "Demonstration designs for the remediation of space debris from the International Space Station," *Acta Astronaut.,* **112**, 102-113 (2015)

[34] L. Daniault, M. Hanna, L. Lombard, Y. Zaouter, E. Mottay, D. Goular, P. Bourdon, F. Druon and P. Georges, "Coherent beam combining of two femtosecond fiber chirped-pulse amplifiers," *Opt. Lett.* **36** (5), 621-623 (2011)

[35] F. di Teodoro, "Pulsed Fiber Lasers," chapter 16, pp. 463-498 in *High Power Laser Handbook*, McGraw Hill (2011)

[36] J. Bourdorionnet, C. Bellanger, J. Primot and A. Brignon, "Collective coherent phase combining of 64 fibers," *Opt. Express* **19** (18) 17053-17059 (2011)

[37] A. Klenke, S. Breitkopf, M. Kienel, T. Gottschall, T. Eidam, S. Hädrich, J. Rothhardt, J. Limpert and A. Tünnermann, "530W, 1.3mJ, four-channel coherently combined femtosecond laser chirped-pulse amplification system," *Opt. Lett.*, **38** (13) 2283-2285 (2013)

[38] C. Phipps, C. Bonnal, F. Masson, M. Boustie, L. Berthe, S. Baton, E. Brambrink, J.-M. Chevalier, L. Videau, S. Boyer and M. Schneider, "Small payload transfers from earth to LEO and LEO to interplanetary space using lasers," paper 679, 7th European Conference for Aeronautics and Space Sciences, Milan (2017)

[39] http://www.hilase.cz/en/advanced-dpssl-laser-dipole-100-delivers-1kw-performance/

[40] http://www.eosenergystorage.com/technology-and-products/, page 2

[41] C. Phipps, G. Albrecht, H. Friedman, D. Gavel, E. George, J. Murray, C. Ho, W. Priedhorsky, M. Michaelis and J. Reilly, "ORION: Clearing near-Earth space debris using a 20kW, 530nm, Earth-based, repetitively pulsed laser," *Laser and Particle Beams* **14**(1) , 1-44 (1996)

[42] C. Phipps, K. Baker, S. Libby, D. Liedahl, S. Olivier, L. Pleasance, A. Rubenchik, J. Trebes, E. George, B. Marcovici, J. Reilly and M. Valley, "Removing orbital debris with lasers," *Adv. Space Resch.* **49**, 1283-1300 (2012)

[43] C. Phipps, J. Reilly and J. Campbell, "Optimum parameters for laser-launching objects into low Earth orbit," *Laser and Particle Beams*, **18**(4) 661-695 (2000)

[44] C. R. Phipps, "L'ADROIT – A spaceborne ultraviolet laser system for space debris clearing," *Acta Astron.* **104**, 243-255 (2014)

[45] C. R. Phipps and C. Bonnal, "A spaceborne, pulsed UV laser system for re-entering or nudging LEO debris, and re-orbiting GEO debris," *Acta Astron.* **118**, 224-236 (2016)

[46] C. Phipps, C. Bonnal, F. Masson, M. Boustie, L. Berthe, S. Baton, E. Brambrink, J.-M. Chevalier, L. Videau and S. Boyer, "Transfers from earth to LEO and LEO to interplanetary space using lasers," *Acta Astron.* (submitted)

[47] J. Ihlemann, F. Beinhorn, H. Schmidt, K. Luther, J. Troe, "Plasma and plume effects on UV laser ablation of polymers," SPIE **5448** (2004) 572–580.

[48] L. N. Myrabo, D. G. Messitt and F. B. Mead Jr., "Ground and flight tests of a laser propelled vehicle," paper AIAA 98-1001, 36th AIAA Aerospace Science Meeting & Exhibit, 12-15 January 1998, Reno, NV (1998)

[49] C. Phipps and J. Luke, "Laser space propulsion – applications at two extremes of laser power," in *Laser Ablation and its Applications,* C. Phipps, ed., Springer Series in Optical Sciences, **129**, Springer, New York (2007), pp. 407-434

[50] J. Sinko and C. Phipps, "Modeling $CO_2$ laser ablation impulse of polymers in vapor and plasma regimes," *Appl. Phys. Lett.,* **95**, 131105-1 to 131105-3 (2009)

[51] A. P. Papavlu, L. Urech, T. Lippert, C. Phipps, J. Hermann and A. Wokaun, "fs Laser-induced Plasmas from Energetic Polymers: Towards Micro-Laser Plasma Thruster Application," *Plasma Process. Polym.* **13** 611-622 (2016)

[52] C. Phipps, "An Alternate Treatment of the Vapor-Plasma Transition," *Int. J. Aero. Innovations* **3**, 45-50 (2011)

[53] The SESAME equation-of-state database is maintained by group T-1 at Los Alamos National Laboratory (sesame@lanl.gov); see S.P. Lyon and J.D. Johnson, "SESAME: The Los Alamos National Laboratory Equation of State Database," LANL Report No. LA-UR-92-3407, 1992 for additional information.

[54] C. Phipps, R. Harrison, T. Shimada, G. York, T. Turner, X. Corlis, H. Steele, L. Haynes and T. King, "Enhanced Vacuum Laser-impulse Coupling by Volume Absorption at Infrared Wavelengths", *Laser and Particle Beams,* **8**, 281 (1990)

[55] C. Phipps and R. Dreyfus, "Laser ablation and plasma formation" in *Laser Ionization Mass Analysis,* Akos Vertes, Renaat Gijbels and Fred Adams, eds., Chemical Physics Monographs **124**, pp. 369-441 (1993)

[56] C. Phipps and J. Luke, paper IEPC 319, International Electric Propulsion Conference, Princeton October 30, 2015 [Figure 5]

[57] B. Poling, J. Prausnitz and J. O'Connell, *The Properties of Gases and Liquids*, 5th edition, McGraw-Hill, New York, 2001, 7.9-7.11

[58] J. Sinko and C. Phipps, "Modeling $CO_2$ laser ablation impulse of polymers in vapor and plasma regimes," *Appl. Phys. Lett.* **95**, 131105, 2009

[59] C. Phipps, J. Reilly and J. Campbell, "Optimum parameters for laser-launching objects into low Earth orbit," *Laser and Particle Beams*, **18**(4), 661-695 (2000)

[60] L. Barker and R. Hollenbach, "Interferometer technique for measuring the dynamic mechanical properties of materials," Review of Scientific Instruments, **36** (11), p.1617-1620. (1965)

[61] M. Durand and P. Laharrague, "System of velocity measurement of a projectile using a Fabry-Pérot interferometer," Proc. Ninth International Congress on H.S Photographic Society of Motion Picture and Television Engineers (1970)

[62] O. T. Strand, D. R. Goosman, C. Martinez, T. L. Whitworth and W. W. Kuhlow, "Compact system for high-speed velocimetry using heterodyne techniques", Review of Scientific Instruments, **77**(8) 083108 (2006)

[63] P. Mercier, J. Benier, A Azzolina, J-M. Lagrange and D. Partouche, "Photonic Doppler velocimetry in shock physics experiments," *Journal De Physique IV*, **134**, 805-812(2006)

[64] S. Bardy, B. Aubert, L. Berthe, P. Combis, D. Hébert, E. Lescoute, J.-L. Rullier and L. Videau, "Numerical study of laser ablation on aluminum for shock-wave applications: development of a suitable model by comparison with recent experiments," *Opt. Eng.* **56** (1), 011014 (2017)

[65] E. Palik, "Handbook of Optical Constants of Solids," E. D. Palik, ed. *Academic,* New York (1985)

[66] S. Atzeni and J. Meyer-Ter-Vehn, "The Physics of Inertial Fusion," S. Atzeni and J. Meyer-Ter-Vehn, eds., *Oxford University Press* (2004)

[67] M. Povarnitsyn, N. Andreev, P. Levashov, K. Khishchenko and O. Rosmej, "Dynamics of thin metal foils irradiated by moderate-contrast high intensity laser beams," *Phys. Plasmas* **19**, 0231101-8; doi: 10.1063/1.3683687

[68] S. Anisimov, G. Kapeliovich and T. Perel'man, "Electron emission from metal surfaces exposed to ultrashort laser pulses," *Sov. Phys. JETP* **39**, 375-377 (1974)

[69] M. Povarnitsyn, N. Andreev, E. Apfelbaum, T. Itina, K. Khishchenko, O. Kostenko, P. Levashov and M. Veysman, "A wide range model for simulation of pump-probe experiments with metals," *Appl. Surf. Sci* **258**, 9480-9483 (2012); doi: 10.1016/ j.apsusc.2011.07.017

[70] S. Scharring, R.-A. Lorbeer and H.-A. Eckel, "Numerical Simulations on Laser-Ablative Micropropulsiomn with Short and Ultrashort Laser Pulses," *Trans. JSASS Aerospace Tech.* **14**(ists30), Pb_ 69-Pb_75 (2016). Doi: 10.2322/tastj.14.Pb_69